October 1996 • NREL/SR-520-21964

Amorphous Silicon Research: Phase II

Annual Technical Progress Report 1 August 1995 - 31 July 1996

S. Guha
United Solar Systems Corporation
Troy, Michigan

National Renewable Energy Laboratory
1617 Cole Boulevard
Golden, Colorado 80401-3393
A national laboratory of
the U.S. Department of Energy
Managed by Midwest Research Institute
for the U.S. Department of Energy
under Contract No. DE-AC36-83CH10093

NREL/SR-520-21964 • UC Category: 1262 • DE96014327

Amorphous Silicon Research: Phase II

Annual Technical Progress Report 1 August 1995 - 31 July 1996

S. Guha
United Solar Systems Corporation
Troy, Michigan

NREL technical monitor: K. Zweibel

National Renewable Energy Laboratory
1617 Cole Boulevard
Golden, Colorado 80401-3393
A national laboratory of
the U.S. Department of Energy
Managed by Midwest Research Institute
for the U.S. Department of Energy
under Contract No. DE-AC36-83CH10093

Prepared under Subcontract No. ZAN-4-13318-02
October 1996

This publication was reproduced from the best available camera-ready copy submitted by the subcontractor and received no editorial review at NREL.

NOTICE

This report was prepared as an account of work sponsored by an agency of the United States government. Neither the United States government nor any agency thereof, nor any of their employees, makes any warranty, express or implied, or assumes any legal liability or responsibility for the accuracy, completeness, or usefulness of any information, apparatus, product, or process disclosed, or represents that its use would not infringe privately owned rights. Reference herein to any specific commercial product, process, or service by trade name, trademark, manufacturer, or otherwise does not necessarily constitute or imply its endorsement, recommendation, or favoring by the United States government or any agency thereof. The views and opinions of authors expressed herein do not necessarily state or reflect those of the United States government or any agency thereof.

Available to DOE and DOE contractors from:
Office of Scientific and Technical Information (OSTI)
P.O. Box 62
Oak Ridge, TN 37831
Prices available by calling (423) 576-8401

Available to the public from:
National Technical Information Service (NTIS)
U.S. Department of Commerce
5285 Port Royal Road
Springfield, VA 22161
(703) 487-4650

Printed on paper containing at least 50% wastepaper, including 20% postconsumer waste

Preface

This Annual Technical Progress Report covers the work performed by United Solar Systems Corp. for the period 1 August 1995 to 31 July 1996 under DOE/NREL Subcontract No. ZAN-4-13318-02. The following personnel participated in the research program.

A. Banerjee, E. Chen, T. Glatfelter, S. Guha (Principal Investigator), H. Laarman, M. Haag, G. Hammond, K. Hoffman, M. Hopson, T. Palmer, S. Sugiyama, D. Wolf, X. Xu, J. Yang, and K. Younan.

Experiments on the back reflector reported in Section 2 were carried out at Harvard University in collaboration with Prof. R. Gordon. We thank him for the collaborative effort. We would like to thank V. Trudeau for preparation of this report.

Executive Summary

Objectives

The principal objective of this R&D program is to expand, enhance and accelerate knowledge and capabilities for the development of high-performance, two-terminal multijunction hydrogenated amorphous silicon (a-Si:H) alloy cells and modules. The near-term goal of the program is to achieve 12% stable active-area efficiency using the multijunction approach.

Approach

The major effort of this program is to develop high efficiency component cells and incorporate them in the triple-junction structure to obtain the highest stable efficiency. New and improved deposition regimes were investigated to obtain better cell performance. Fundamental studies to obtain better understanding of material and cell performance were undertaken.

Status/Accomplishments

- In order to facilitate optimum ion bombardment during growth, a large parameter space involving chamber pressure, rf power and hydrogen dilution were investigated. No further improvement in cell efficiency could be obtained in this expanded parameter space.

- Replacing hydrogen with deuterium in the intrinsic layer is found to improve cell stability against light exposure. The deuterated alloys are believed to have a different structure from that of the hydrogenated alloy.

- The *template* effect was investigated by making cells on thin and thick *n*-type layers. The results do not show any difference in cell performance.

- The incorporation of a microcrystalline *n* layer in a multijunction cell is seen to improve cell performance.

- State-of-the-art component cells show the following initial active-area performance. Top cell on stainless steel: V_{oc} = 1.054 V, J_{sc} = 6.2 mA/cm^2, FF = 0.76 and P_{max} = 5.0 mW/cm^2. This is the highest V_{oc} of a high quality a-Si alloy single-junction cell reported in the literature. Middle cell on back reflector: V_{oc} = 0.79 V, J_{sc} = 21.24 mA/cm^2, FF = 0.646 and P_{max} = 10.84 mW/cm^2. This is the highest efficiency reported for a-SiGe alloy solar cell. Bottom cell on a back reflector and measured under AM 1.5 illumination with a cut-on filter of wavelength greater than 630 nm: V_{oc} = 0.59 V, J_{sc} = 12.5 mA/cm^2, FF = 0.63 and P_{max} = 4.64 mW/cm^2. This is also the highest power output from the bottom cell reported in the literature.

- Triple-junction cells have been fabricated, demonstrating the world's highest stable active-area efficiency of 11.83%. This a major improvement over the previous highest efficiency of 11.1% reported during Phase I of this program.

Table of Contents

		Page
Preface		**1**
Executive Summary		**2**
Table of Contents		**3**
List of Figures		**5**
List of Tables		**7**
Section 1	**Introduction**	**8**
Section 2	**Effects of Buffer Layer on Back Reflector Performance**	**9**
	Introduction	**9**
	Effect of Titanium Oxide Layer Between ZnO and a-Si Alloy	**9**
	Effect of Magnesium Fluoride Layer Between Ag and ZnO	**13**
Section 3	**Effect of Deposition Parameters on a-Si:H Solar Cells**	**15**
	Introduction	**15**
	Results and Discussion	**15**
Section 4	**Stability of a-Si:D vs. a-Si:H *p i n* Cells**	**19**
	Introduction	**19**
	Results and Discussion	**19**
Section 5	**Effect of *n* Layer Thickness on Cell Performance**	**21**
	Introduction	**21**
	Results and Discussion	**21**
Section 6	**Effect of µc-*n* Layer on a-Si:H/a-Si:H and a-Si:H/ a-SiGe:H Double-junction Cells**	**25**
	Introduction	**25**
	Effect of Microcrystalline *n* Layer in the Tunnel Junction of *n i p n* and $n_1 i_1 p_1 n_2 i_2 p_2$ Structure	**25**
	Effect of Microcrystalline *n* Layer in the Tunnel Junction of Double-junction Cells	**27**

		Page
Section 7	**Status of Component Cells and Triple-junction Performance**	**32**
	Introduction	**32**
	Experimental Results and Discussion	**32**
Section 8	**Future Directions**	**42**
References		**43**

List of Figures

		Page
1.	Reflectivity versus wavelength for four substrates described in the text.	10
2.	Quantum efficiency and reflectivity curves versus wavelength for four a-SiGe:H solar cells on the four substrates in Fig. 1.	11
3.	Sum of quantum efficiency and reflectivity curves versus wavelength for the four samples in Fig. 2.	12
4.	Reflection versus wavelength of the incident light for two back reflector structures described in the text.	14
5.	Red (open circle) and white (solid circle) fill factors of a-Si:H solar cells versus intrinsic layer thickness.	16
6.	Red (open circle) and white (solid circle) fill factors of a-Si:H solar cells versus applied bias voltage.	17
7.	Red (open circle) and white (solid circle) fill factors of a-Si:H solar cells versus chamber pressure.	18
8.	Normalized fill factor versus light-soaking time for two a-Si:H solar cells with thin and thick *n* layers.	23
9.	(a) Quantum efficiency of two degraded a-Si:H solar cells with thin and thick *n* layers and (b) ratio of initial to degraded quantum efficiency of the two cells.	24
10.	Quantum efficiency versus wavelength of an a-Si:H/a-Si:H double-junction cell (L8314) with amorphous *n* layer in the tunnel junction.	28
11.	Quantum efficiency versus wavelength of an a-Si:H/a-Si:H double-junction cell (L8317) with microcrystalline *n*/buffer combination in the tunnel junction.	29
12.	Quantum efficiency versus wavelength of an a-Si:H/a-SiGe:H double-junction cell (L8375) with amorphous *n* layer in the tunnel junction.	30
13.	Quantum efficiency versus wavelength of an a-Si:H/a-SiGe:H double-junction cell (L8376) with microcrystalline *n*/buffer combination in the tunnel junction.	31
14.	Schematic diagram of triple-junction triple-bandgap device.	34

Page

15. Quantum efficiency of a-SiGe alloy (a) bottom cell and (b) middle cell deposited on back reflector. 35

16. P_{max} versus light-soaking time for an a-SiGe:H narrow bandgap cell with a stabilized P_{max} = 3.80 mW/cm^2. 36

17. Initial J-V characteristic of an a-SiGe alloy middle cell deposited on back reflector. 37

18. Initial J-V characteristic of a top cell on ss. 39

19. Stabilized J-V characteristic of the 11.8% cell. 40

20. Quantum efficiency of the triple cell in Fig. 19. 41

List of Tables

		Page
1.	J-V Characteristics of a-SiGe:H *p i n* Solar Cells on Four Back Reflectors Measured under AM1.5 Illumination with a λ>630 nm Cut-on Filter.	9
2.	Integrated Short-circuit Currents of the Structures Described in the Text.	13
3.	Initial and Light-soaked J-V Characteristics for *p i n* Solar Cells Deposited on ss with Intrinsic Layers using SiH_4/H_2 and SiD_4/D_2 Mixtures.	19
4.	Initial and Light-soaked J-V Characteristics for Three *p i n* Cells on ss with Different Gas Mixtures.	20
5.	Characteristics of Two a-Si:H Cells Deposited on *n* Layers with Different Thicknesses.	22
6.	Characteristics of Two a-Si:H Cells Deposited on *n* Layers with Different Thicknesses.	22
7.	J-V Characteristics of $n_1i_1p_1n_2$ Structures.	26
8.	Characteristics of a-Si:H/a-Si:H $n_1i_1p_1n_2i_2p_2$ Double-junction Structures.	26
9.	Q_{550} Characteristics of $n_1i_1p_1n_2$ Structures.	27
10.	Characteristics of Double-junction Cells with Amorphous and Micro-crystalline/Buffer *n* Layers in the Tunnel Junction.	27
11.	Initial and Degraded Characteristics of Two Earlier Triple-junction Cells.	33
12.	J-V Characteristics of the Previous, Recent, and Present Bottom Cells Deposited on Back Reflector and Measured under AM1.5 Illumination with a λ>630 nm Filter.	33
13.	Characteristics of Improved Triple-junction Cells with Enhanced Current Mismatch.	38

Section 1

Introduction

This report describes the research performed during Phase II of a three-phase, three-year program under NREL Subcontract No. ZAN-4-13318-02. The research program is intended to expand, enhance and accelerate knowledge and capabilities for the development of high-performance, two-terminal multijunction hydrogenated amorphous silicon (a-Si:H) alloy modules.

It is now well recognized that a multijunction, multibandgap approach has the potential of achieving the highest stable efficiency in a-Si:H alloy solar cells. In this approach, the bandgap of the materials of the component cell is varied in order to capture a wide spectrum of the solar photons. Significant progress has been made in the development of materials and cell design in the last few years, and a stable module efficiency of 10.2% has been demonstrated over one-square-foot area using a triple-junction approach in which the bottom two component cells use hydrogenated amorphous silicon-germanium (a-SiGe:H) alloy. In order to meet the Department of Energy goal of achievement of 12% stable module efficiency, it is necessary to make further improvements in each of the component cells. This has been the thrust of the current program.

One of the key factors which can improve the performance of amorphous silicon (a-Si) alloy solar cells is the design of a suitable back reflector which will facilitate light trapping. Although significant progress has been made by using silver/zinc oxide back reflector, there is a scope for improvement if the loss between silver and zinc oxide (ZnO) or ZnO and silicon could be minimized. In collaboration with Prof. Roy Gordon's group at Harvard University, we have studied the effect of introducing a layer of niobium-doped titanium oxide on cell performance. We have also investigated the effect of a layer of MgF_2 on cell performance. The results are presented in Section 2.

It is well recognized that plasma chemistry, choice of suitable precursors, and growth kinetics affect the material properties. In Section 3, we present results on the effect of plasma chemistry on a-Si alloy cell performance where the chemistry is altered by changing chamber pressure, rf power, substrate temperature and hydrogen dilution. In Section 4, we describe our efforts to replace hydrogen with deuterium in the plasma and the effect on cell performance. In Section 5, we investigate the *template* effect by comparing performance of cells in which the intrinsic layers are grown on thick or thin *n*-type layers.

The tunnel junction between the doped layers in a multijunction cell plays an important role in determining cell performance. In Section 6, we discuss the effect of the incorporation of a microcrystalline *n*-type layer in the tunnel junction on multijunction cell performance.

In Section 7, we summarize the status of our component cells and the triple-junction structures and report on the achievement of a new world record of 11.83% stable cell efficiency. All cell efficiency numbers quoted in this report are based on active-area measurements. Future directions are outlined in Section 8.

Section 2

Effect of Buffer Layer on Back Reflector Performance

Introduction

One of the key factors which can improve the performance of a-Si alloy solar cell is the design of a suitable back reflector which will facilitate light trapping by total internal reflection. We have demonstrated significant increase in the short-circuit current density by the use of a textured Ag/ZnO back reflector. A careful analysis of the data, however, reveals (Guha 1993) that there may be parasitic losses associated with Ag/ZnO and/or ZnO/a-Si alloy interface. In order to study the effect of incorporating an additional buffer layer between ZnO and a-Si alloy, we have sent three ss/Ag/ZnO back reflectors to Prof. Roy Gordon of Harvard University for APCVD deposition of niobium doped titanium oxide. The motivation is to investigate if the titanium oxide layer would reduce parasitic loss and result in higher short-circuit current.

Effect of Titanium Oxide Layer Between ZnO and a-Si Alloy

Figure 1 plots reflectivity measurements of four substrates versus wavelength. Substrate #1 is the control substrate which is our standard ss/Ag/ZnO back reflector, while substrates #2, #3, and #4 are standard ss/Ag/ZnO back reflectors coated with different thicknesses of titanium oxide. It should be pointed out that the reflectivity of titanium oxide coated back reflectors for samples #2 and #3 is higher than the control back reflector for long wavelengths.

We then proceeded to deposit narrow bandgap a-SiGe:H solar cells on these four substrates under identical conditions. Figure 2 plots the quantum efficiency and reflectivity curves versus wavelength for the four samples. It is observed that the control sample has the highest current for λ>630 nm. The additional titanium oxide layer apparently did not reduce any parasitic loss of the ZnO/a-Si alloy interface. Figure 3 plots the sum of quantum efficiency and reflectivity (Q+R) versus wavelength. The Q+R value turned out to be greater for the control sample for the long wavelength region indicating additional optical loss due to titanium oxide.

The J-V characteristics for λ>630 nm are summarized in Table 1. It should be pointed out that while we did not observe any enhancement in J_{sc}, the incorporation of the titanium oxide layer does not introduce any appreciable additional series resistance. We are now planning to study the effect of a titanium oxide layer between Ag and ZnO. We shall also try titanium oxide with different Nb content.

Table I. J-V Characteristics of a-SiGe:H *p i n* Solar Cells on Four Back Reflectors Measured under AM1.5 Illumination with a λ>630 nm Cut-on Filter.

Sample	Substrate	J_{sc} (mA/cm^2)	V_{oc} (V)	FF	P_{max} (mW/cm^2)	R_s (Ω-cm^2)
5008	1	8.72	0.678	0.535	3.16	24
5009	2	7.95	0.693	0.550	3.03	32
5012	3	8.10	0.678	0.512	2.81	30
5013	4	7.92	0.673	0.519	2.77	25

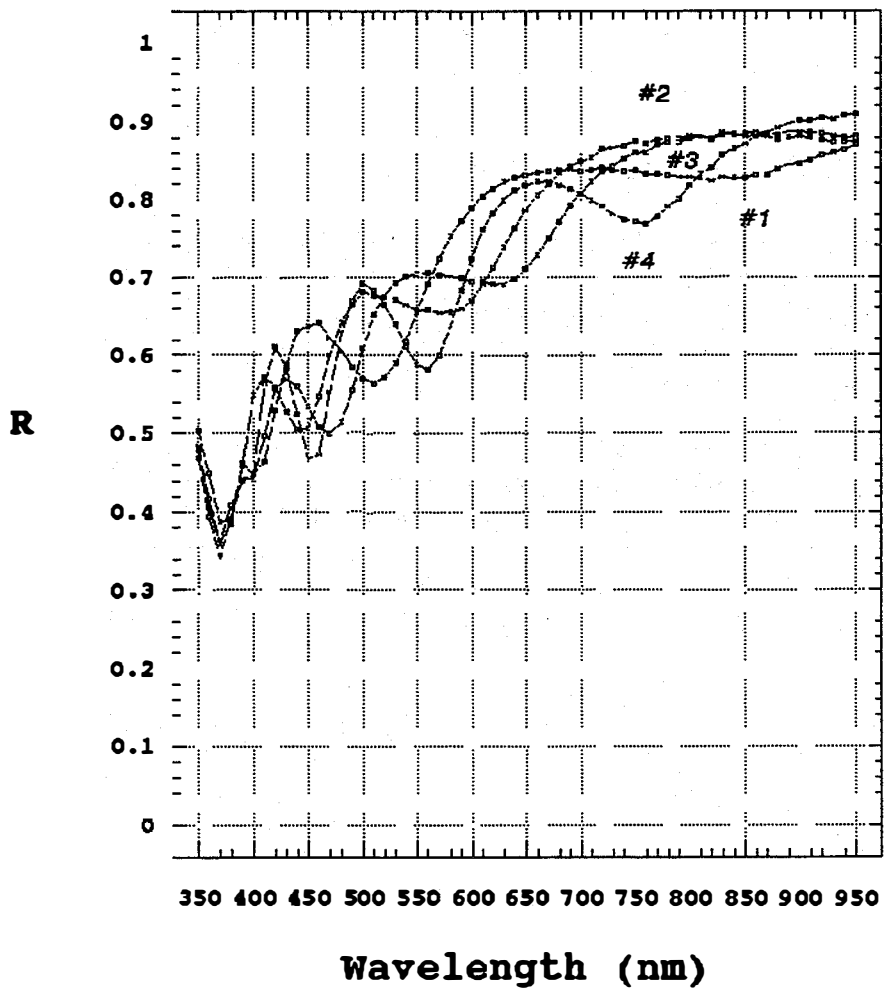

Figure 1. **Reflectivity versus wavelength for four substrates described in the text.**

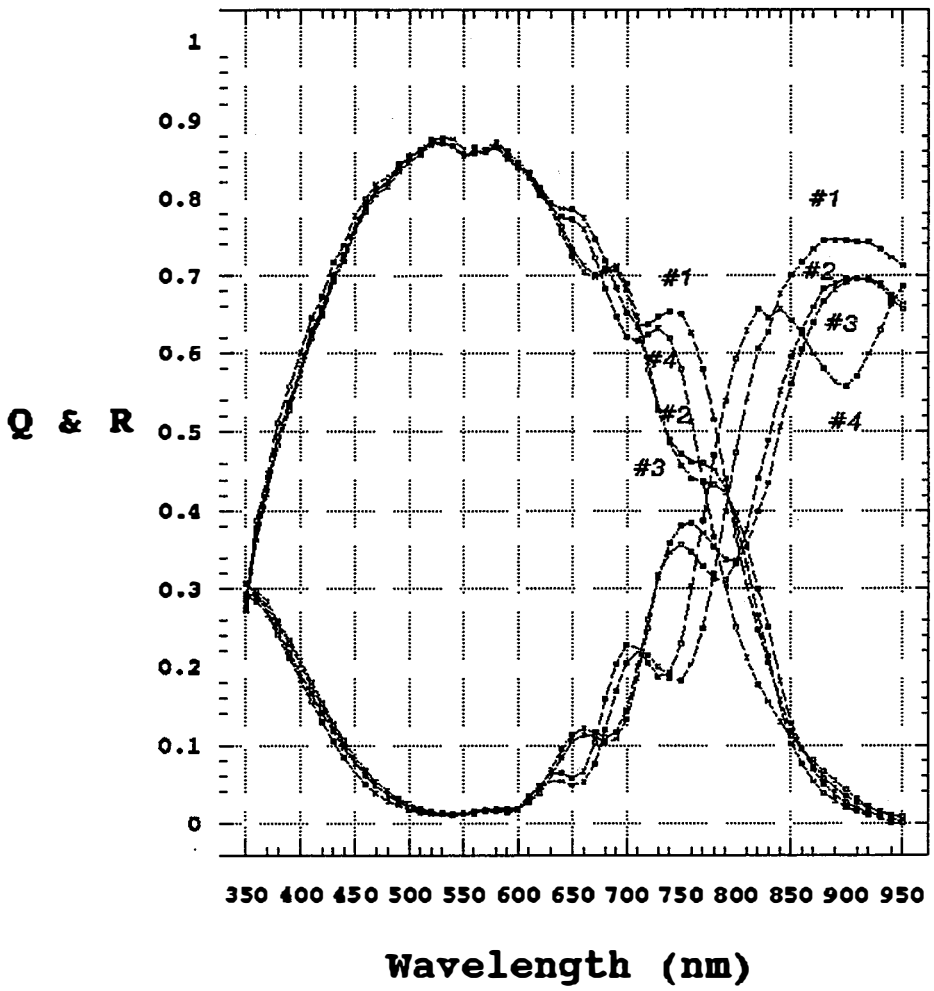

Figure 2. **Quantum efficiency and reflectivity curves versus wavelength for four a-SiGe:H solar cells on the four substrates in Fig. 1.**

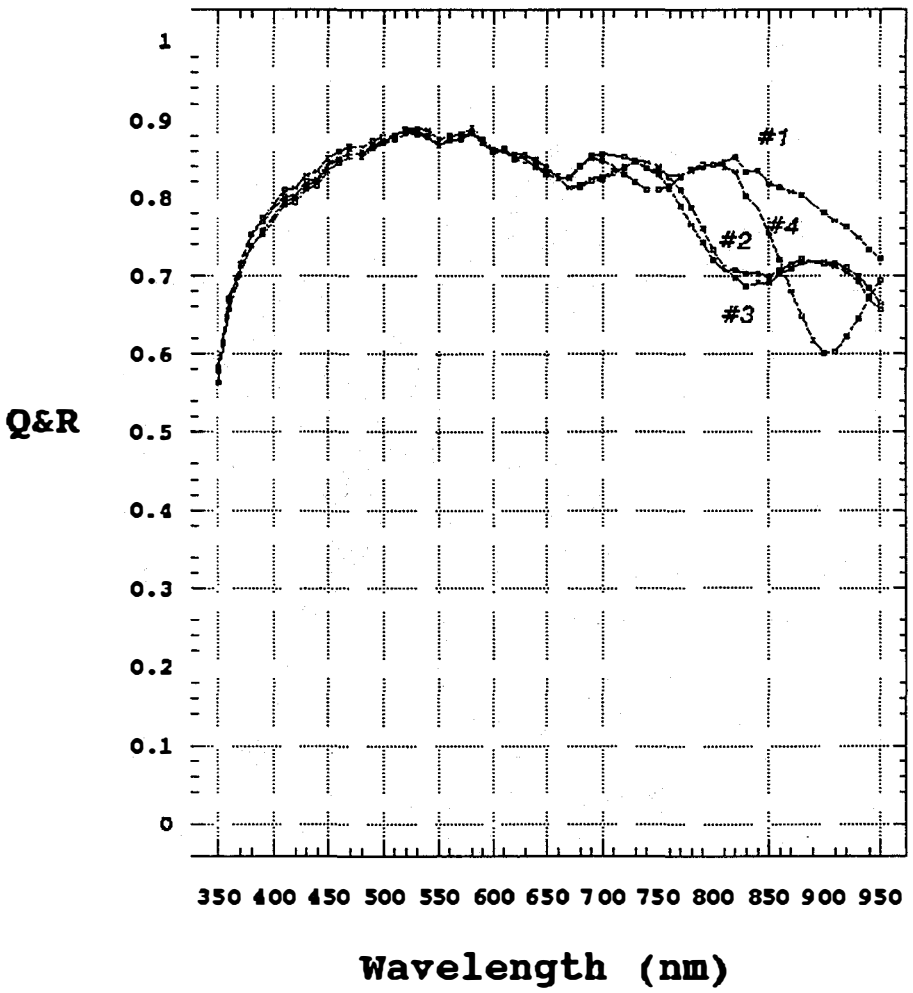

Figure 3. **Sum of quantum efficiency and reflectivity curves versus wavelength for the four samples in Fig. 2.**

Effect of Magnesium Fluoride Layer Between Ag and ZnO

In addition, in our laboratory, we have developed an optically transparent magnesium fluoride (MgF_2). As it is a reasonably dense material, we expect that it would serve as an optical buffer layer. This proved to be the case as illustrated in Fig. 4. This figure displays the reflection dispersion for two structures: a stainless steel substrate coated with our standard BR materials of Ag and ZnO and the same structure but with MgF_2 deposited between the Ag and ZnO depositions. The MgF_2 was grown by thermal evaporation. The film is approximately 3000 Å thick. Notice in Fig. 4 that the effect of the inserted MgF_2 is to improve the reflection. It was our hope that the improvement was due to a repair of a parasitic optical loss at the Ag/ZnO interface. Therefore, we expected an improvement in the optical response of solar cells made on top of this new BR.

Unfortunately, MgF_2 is an electrical insulator. Thus, it is difficult to use as one of the layers in our standard solar cell structures. However, we devised a technique to make working solar cells with the MgF_2 layer as part of the structure. It involves "drilling" microscopic holes into the substrate immediately after the MgF_2 layer is deposited and prior to the ZnO coating. If the holes are appropriately dense, then the holes will conduct the solar cell current with only slight loss and lateral conduction may be provided by the ZnO layer. In our lab, we have a computer controlled apparatus consisting of a precision x-y positioner, an optical alignment system, and a Nb-YAG laser. This equipment was used to "drill" the required holes to provide to us a method of making solar cells using the enhanced structure as seen in Fig. 4.

Identical *n i p* devices of a-SiGe:H were deposited onto each of the substrates of Fig. 4. The spectral response of the cells were measured and integrated with respect to AM1.5 Standard Global Spectrum. The resulting current densities are presented in Table 2. We were disappointed to discover that the new MgF_2 did *not* result in any current enhancement. In this table we also display integrated currents for only wavelengths greater than 630 nm. This integration was performed to eliminate any differences in the spectral response curves due to factors other than the substrate effects. As seen in Table 2, this calculation is consistent with the overall integrated spectral response. Therefore, we must conclude that the MgF_2 did not give any optical enhancement. At present, we do not understand the reason for the reflection data of Fig. 4. We theorize that the interpretation of reflection spectra from textured surfaces where the size of the texture is of the order of the wavelength is not straight forward. We continue to believe that solar cells made using our standard structure are influenced by parasitic optical losses. However, we do not know the extent of the effect of the losses on the short circuit current of solar cells. The two-dimensional model being developed by Bhushan Sopori of National Renewable Energy Laboratory may be able to show further light on these issues.

Table 2. Integrated Short-circuit Currents of the Structures Described in the Text.

Structure	Jsc-AM1.5	Jsc->630nm
Ag/ZnO	21.7 mA/cm^2	9.6 mA/cm^2
Ag/MgF_2/ZnO	21.2 mA/cm^2	9.2 mA/cm^2

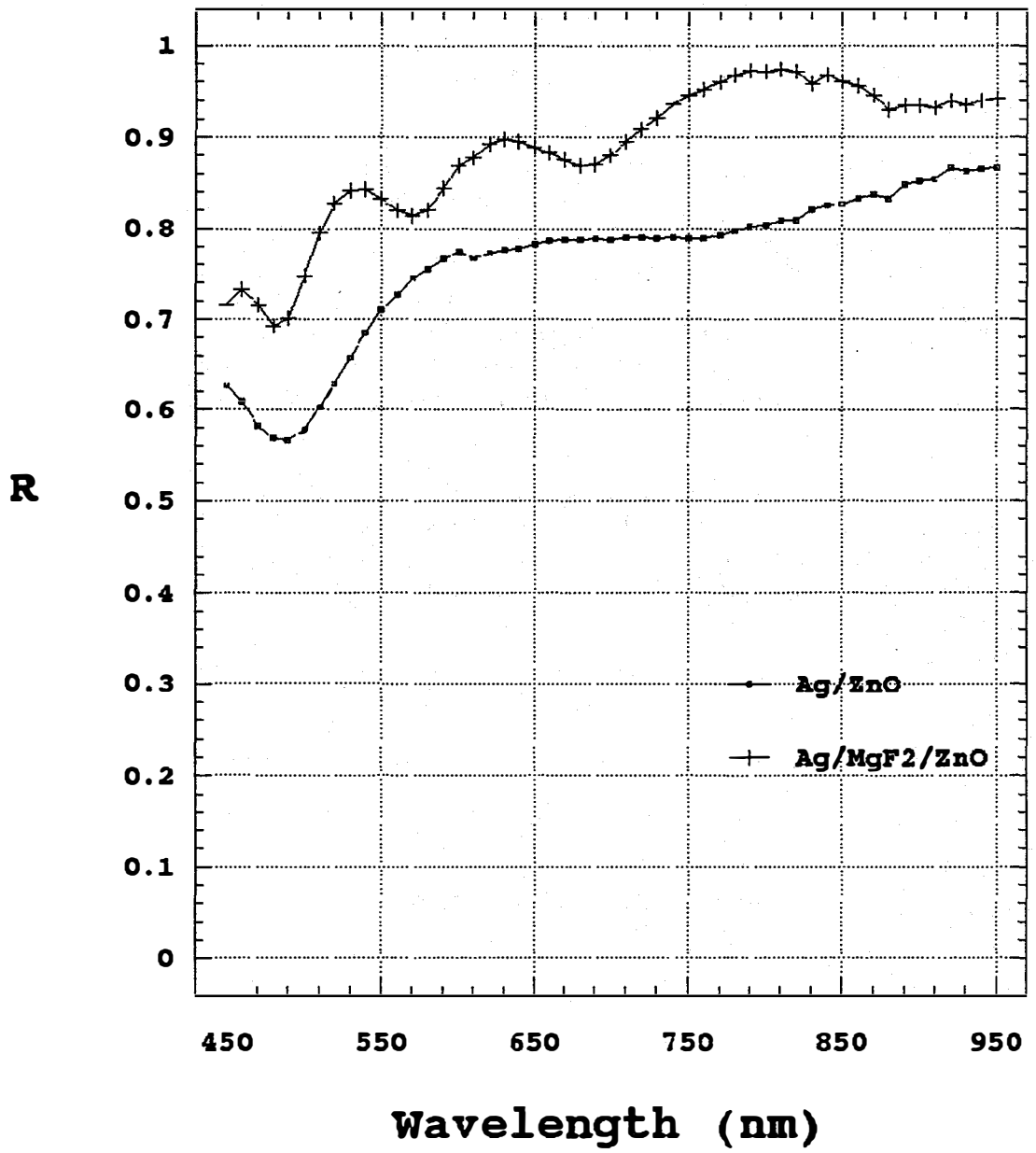

Figure 4. **Reflection versus wavelength of the incident light for two back reflector structures described in the text.**

Section 3

Effect of Deposition Parameters on a-Si:H Solar Cells

Introduction

In our previous report (Guha 1995), we presented the effect of ion bombardment on a-Si:H solar cells by the application of dc bias voltage to the substrate during deposition. Experimental results showed that in the triode mode, positive bias improves the cell performance slightly, while in the diode mode, there is essentially no effect of bias.

Recently, Ganguly and Matsuda carried out an experiment where the plasma potential was controlled by changing deposition parameters such as the applied power, chamber pressure and the spacing between electrodes (Ganguly and Matsuda 1995). They reported that within a narrow range of plasma potential (ion energy), the room temperature hole drift mobility in a-Si:H was enhanced by two orders of magnitude. This would, of course, lead to a tremendous improvement in solar cell performance.

Results and Discussion

We have started a series of experiments on a-Si:H solar cells where we have varied the deposition parameters. The experiments were carried out in a conventional rf plasma-enhanced CVD system having a diode configuration, and the substrate was grounded instead of being floated as in previous dc bias experiments. The following parameters were varied: pressure, rf power and hydrogen dilution. Figure 5 shows both red FF (open circles) and white FF (solid circles) of a-Si:H cells as a function of thickness of the intrinsic layer. As expected, the white FF decreases as the cells get thicker, particularly as thickness exceeds 5500 Å. Note that the scatter in the data is caused by the different deposition conditions.

Dependence of a-Si:H cell performance (for cells with thickness in the range 4600 ± 500 Å) on bias voltage (measured between the cathode and the substrate) and chamber pressure is shown in Figs. 6 and 7, respectively. Although the values of the red FF remain between 0.70 to 0.74, the white FF shows larger fluctuation, scattering from 0.60 to 0.68. The best value of white FF in this group of samples is 0.68, which is comparable to our good baseline value. We thus find that even though we have probed a reasonable range of deposition parameters, we have not been able to achieve the narrow optimum deposition condition under which Ganguly and Matsuda obtained the very high hole mobility.

We note that Ganguly and Matsuda (Ganguly and Matsuda 1995), commented that even under nominally optimal plasma conditions, only about 20% of the samples turned out to be good. Therefore, 16 runs involved in our experiments may not be sufficient to obtain the "extraordinary" results on solar cells.

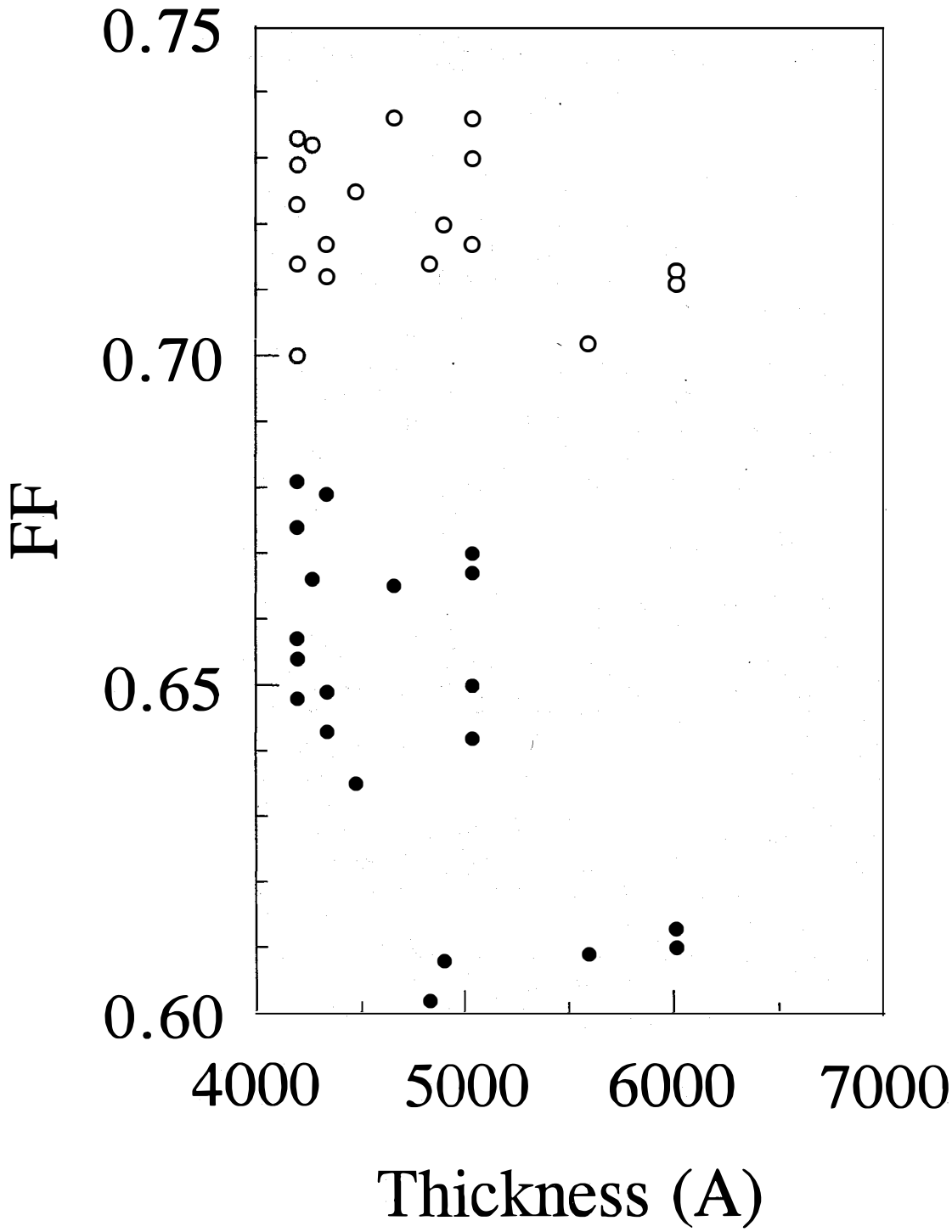

Figure 5. Red (open circle) and white (solid circle) fill factors of a-Si:H solar cells versus intrinsic layer thickness.

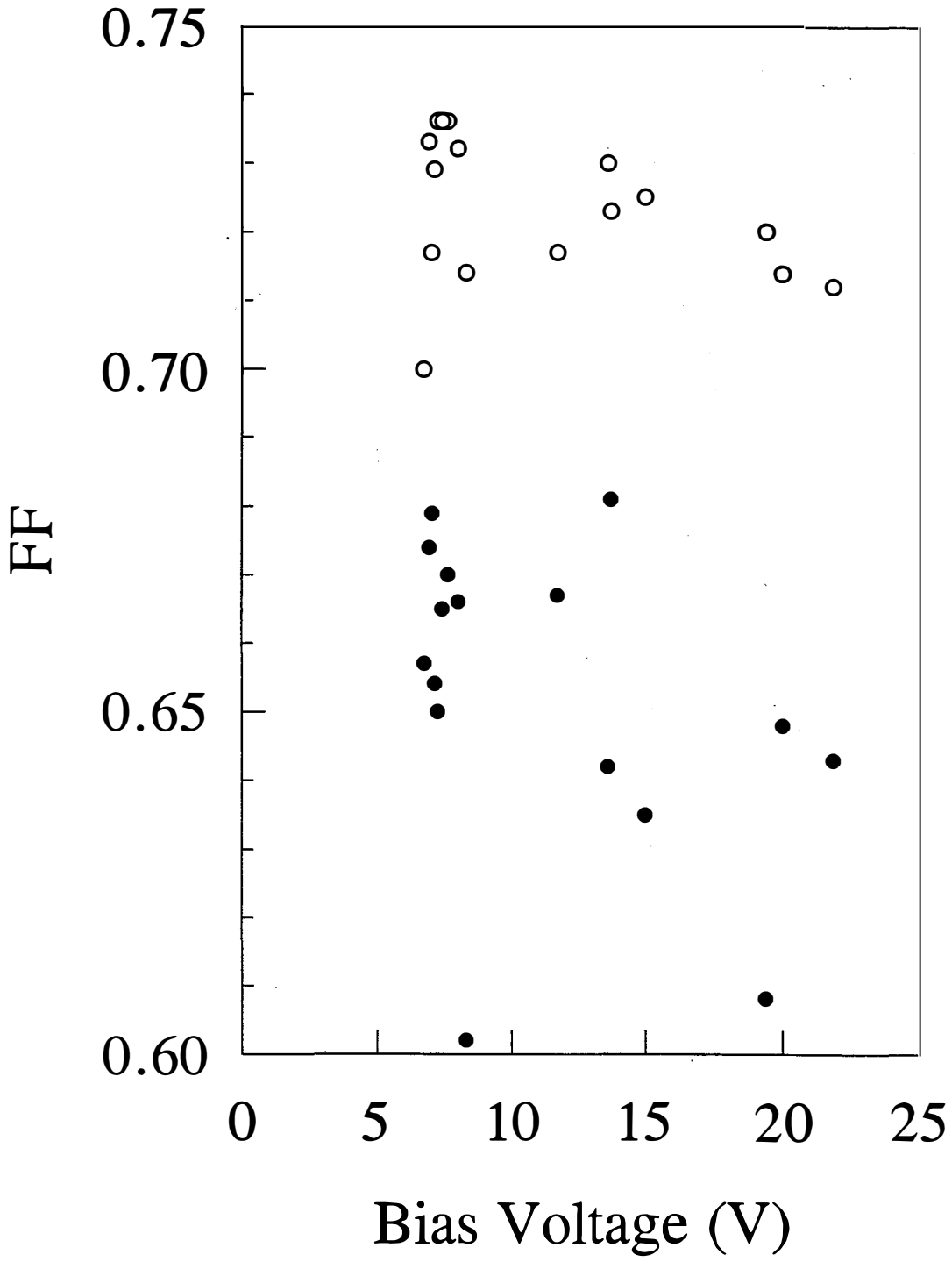

Figure 6. Red (open circle) and white (solid circle) fill factors of a-Si:H solar cells versus applied bias voltage.

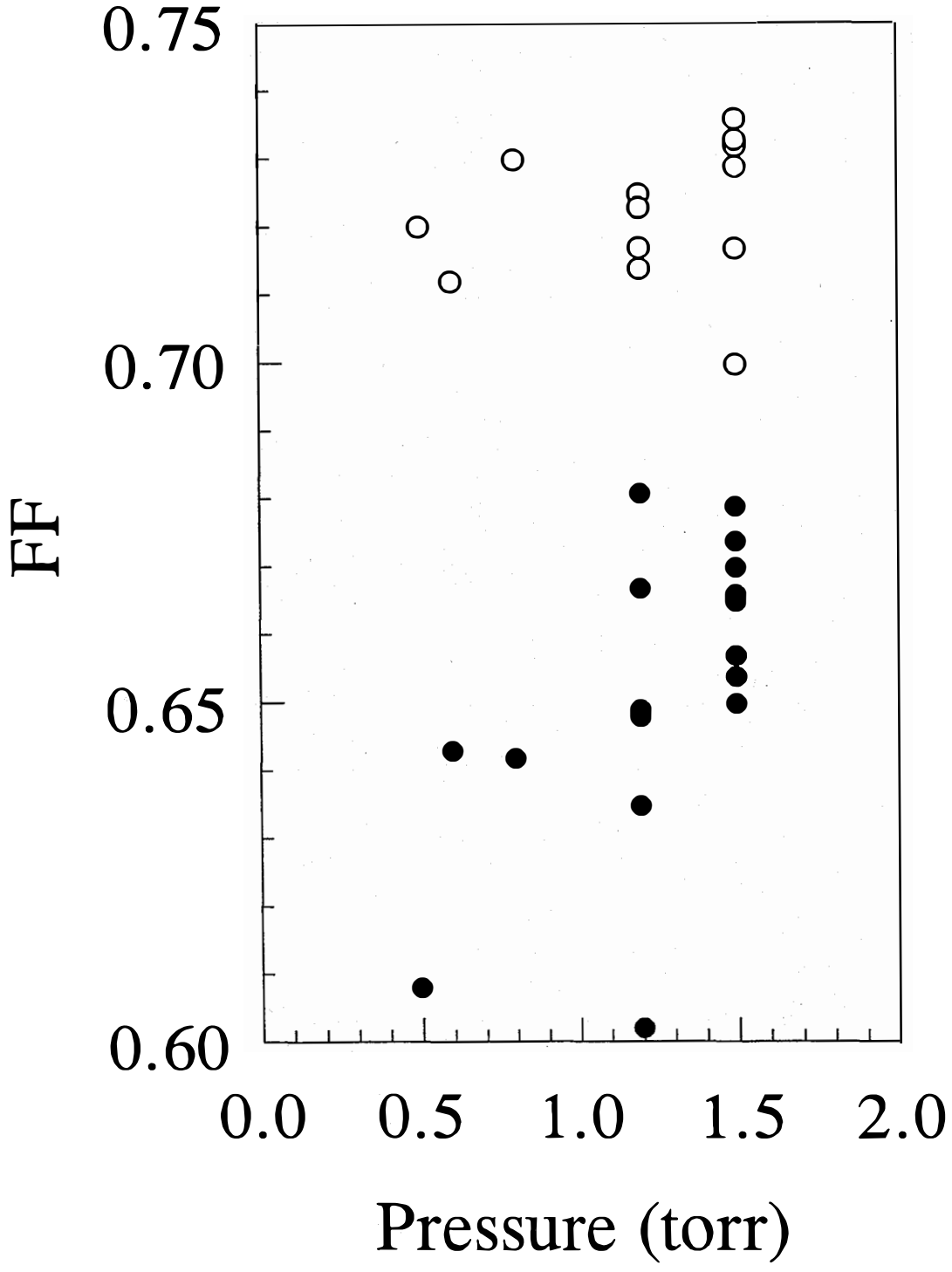

Figure 7. Red (open circle) and white (solid circle) fill factors of a-Si:H solar cells versus chamber pressure.

Section 4

Stability of a-Si:D vs. a-Si:H *p i n* Cells

Introduction

In a recent paper, Lyding, et al. (Lyding at al. 1996) reported on the reduction of hot electron degradation in MOS transistors by deuterium processing. They observed that by replacing hydrogen with deuterium during the final wafer sintering process, transistor lifetime improved by factors of 10 to 50 times.

Comparison of light-induced degradation on hydrogenated and deuterated amorphous silicon alloy films has been reported by Ganguly, et al. (Ganguly et al. 1990, 1991, 1994) and Stutzmann, et al. (Stutzmann et al. 1986). However, information regarding any beneficial effect of deuterium on material quality has been inconclusive.

Results and Discussion

We have conducted two experiments in which we compared solar cell performance between hydrogenated and deuterated solar cells. The first experiment consists of depositing *p i n* solar cells on ss using RF glow discharge in which intrinsic layers are made from SiH_4/H_2 and SiD_4/D_2 mixtures and having a similar thickness. The J-V characteristics for initial and 1000 hr light-soaked values are summarized in Table 3.

Table 3. Initial and Light-soaked J-V Characteristics for *p i n* Solar Cells Deposited on ss with Intrinsic Layers using SiH_4/H_2 and SiD_4/D_2 Mixtures.

Sample	Thickness (nm)	Temp.	Gas Mixture in Intrinsic Layer	Light-Soaked (hour)	J_{sc} (mA/cm^2)	V_{oc} (V)	FF	η (%)
5566	410	275 °C	SiD_4/D_2	0	14.6	0.99	0.63	9.1
				1000	13.7	0.97	0.58	7.7
				Degradation (%)	6.2	2.0	7.9	15.4
5607	420	275 °C	SiH_4/H_2	0	16.7	0.94	0.65	10.2
				1000	15.6	0.91	0.55	7.8
				Degradation (%)	6.6	3.2	15.4	23.6

It is noted that the deuterated cell exhibits a higher V_{oc}; this may be due to higher D-content in the deuterated alloy giving rise to a higher bandgap. This also lowers J_{sc}. Although the initial FF is slightly lower for the deuterated cell, the stabilized FF is higher, showing only a 7.9% degradation in FF as compared to a 15.4% degradation for the hydrogenated cell. The overall degradation is 15.4% for the deuterated cell, much less than the 23.6% for the hydrogenated cell.

In the second experiment, we compared three *p i n* cells with intrinsic layers deposited at 200 °C and having the same thickness. Cell 5742 has all three layers made from SiD_4 and D_2 mixture with dopants added to *p* and *n* layers. Cell 5622 uses SiD_4 and D_2 in the intrinsic layer while the doped layers use SiH_4 and H_2. Cell 5752 uses SiH_4 and H_2 in all the three layers. The initial and 1010-hour, light-soaked J-V characteristics are summarized in Table 4.

Table 4. Initial and Light-soaked J-V Characteristics for Three *p i n* Cells on ss with Different Gas Mixtures.

Sample	Thickness (nm)	Temp.	Gas Mixture in Intrinsic Layer	Light-Soaked (hour)	J_{sc} (mA/cm^2)	V_{oc} (V)	FF	η (%)
5742	310	200 °C	*p,i,n* SiD_4/D_2	0	13.72	0.977	0.678	9.09
				1010	13.30	0.977	0.632	8.21
				Degradation (%)	3.1	0	6.8	9.7
5622	310	200 °C	*p,n* SiH_4/H_2 *i* SiD_4/D_2	0	13.17	1.018	0.704	9.44
				1010	12.91	1.005	0.655	8.50
				Degradation (%)	2.0	1.3	7.0	10.0
5752	310	200 °C	*p,i,n* SiH_4/H_2	0	15.13	0.968	0.676	9.90
				1010	14.46	0.930	0.607	8.16
				Degradation (%)	4.4	3.9	10.2	17.6

One notes from Table 4 that using SiD_4/D_2 mixture in all three layers did not eliminate light-induced degradation. The lower value in V_{oc} for 5742 (all layers deuterated) than for 5622 (only *i* layer deuterated) may be due to the fact that the microcrystalline *p* layer in 5742 is not quite optimized. The degradation in FF, however, for 5742 and 5622 is similar. Comparing deuterated cells with hydrogenated cells, we conclude that deuterated cells are more stable. Further experiments are continuing.

We thank J. Morabito and C. Wronski for bringing the Lyding et al. 1996 reference to our attention.

Section 5

Effect of *n* Layer Thickness on Cell Performance

Introduction

It has been reported that the stability of a-Si:H cells depends significantly on the thickness of the *n* layer in a *p i n*/ss structure (Dalal 1995.) The cell with a thick *n* layer (about 1 µm) showed much better stability than the cell with a thin *n* layer (about 0.1 µm). It was speculated that the quality of the *i* layer improves when it is deposited on a thick *n* layer (because of a *template* effect). We have carried out experiments on a-Si:H cells with different *n* layer thicknesses and did not observe any significant effect on the cell performance.

Results and Discussion

The structure of a-Si:H cells is ss/*n i p*/ITO without back reflectors. Two sets of cells were prepared for this study. For the first set, two samples were made under nominally identical conditions except for the *n* layer thickness. The intrinsic layer is about 450 nm thick. The thicknesses are 1 µm and 20 nm, respectively, for the thick and thin *n* layers.

Photovoltaic characteristics of the two cells are listed in Table 5. It is interesting to note that the thick *n* layer cell shows slightly higher FF than the thin *n* layer cell while the latter has a slightly higher J_{sc}. This is due to a small amount of back reflection from ss for λ>550 nm for the thin *n* layer cell.

The two samples were exposed to one-sun white light at 50 °C in open-circuit mode for up to 620 hours. The normalized FF's are plotted in Fig. 4 as a function of light-soaking time. It is clear that both cells show very similar light-induced degradation behavior. The degradation in cell efficiency is 17~18%, and both cells show a tendency of saturation after 200 hours of light soaking.

In order to exclude any difference that may be introduced by run-to-run variation, we have prepared a second set of samples in a different way. A thick *n* layer was first deposited on one-half of the substrate, while the other half of the substrate was covered. The substrate was then exposed to air and the cover removed. Thin *n, i,* and *p* layers were subsequently deposited onto the entire substrate on which one-half has a thick *n* layer. The thicknesses of the thick and thin *n* layers were approximately 1 µm and 20 nm, respectively. The *i* layer is approximately 400 nm thick.

The characteristics of the second set of the samples are summarized in Table 6 for both the initial and degraded states. Except for the fact that the cell with thin *n* layer shows a slightly higher J_{sc}, there is no appreciable difference in the cell performance between the cells with thick and thin *n* layers in both the initial and degraded states.

The quantum efficiency (Q) data of the two degraded devices of L7925 are shown in Fig. 9a. It is clear that Q's in the short wavelength region are overlapping on each other; in the long wavelength region, the device with the thin *n* layer shows a slightly higher Q due to the small amount of reflection from the ss. The ratio of the initial Q to the degraded Q is illustrated in Fig. 9b. It is noted that Q degraded by the same amount for the two devices. Dalal (Dalal 1995) reported much less degradation in Q in the cell with a thick *n* layer.

In summary, we did not observe any appreciable difference in the cell performance for both the initial and light-soaked states for different *n* layer thicknesses on the ss/*n i p*/ITO structure.

Table 5. Characteristics of Two a-Si:H Cells Deposited on *n* Layers with Different Thicknesses.

Sample #	State	J_{sc} (mA/cm^2)	V_{oc} (V)	FF	P_{max} (mW/cm^2)
2081	Initial	12.4	0.96	0.63	7.45
Thick *n*	620 hour	11.6	0.93	0.57	6.13
2085	Initial	13.0	0.95	0.60	7.46
Thin *n*	620 hour	12.3	0.92	0.55	6.20

Table 6. Characteristics of Two a-Si:H Cells Deposited on *n* Layers with Different Thicknesses. The *i* and *p* layers of two cells were deposited in the same run.

Sample #	State	J_{sc} (mA/cm^2)	V_{oc} (V)	FF_w	FF_{red}	P_{max} (mW/cm^2)
7925/31	Initial	12.2	0.94	0.65	0.73	7.4
Thin *n*	500 hour	11.9	0.92	0.60	0.60	6.5
7925/34	Initial	11.8	0.94	0.65	0.73	7.2
Thick *n*	500 hour	11.5	0.92	0.60	0.60	6.4

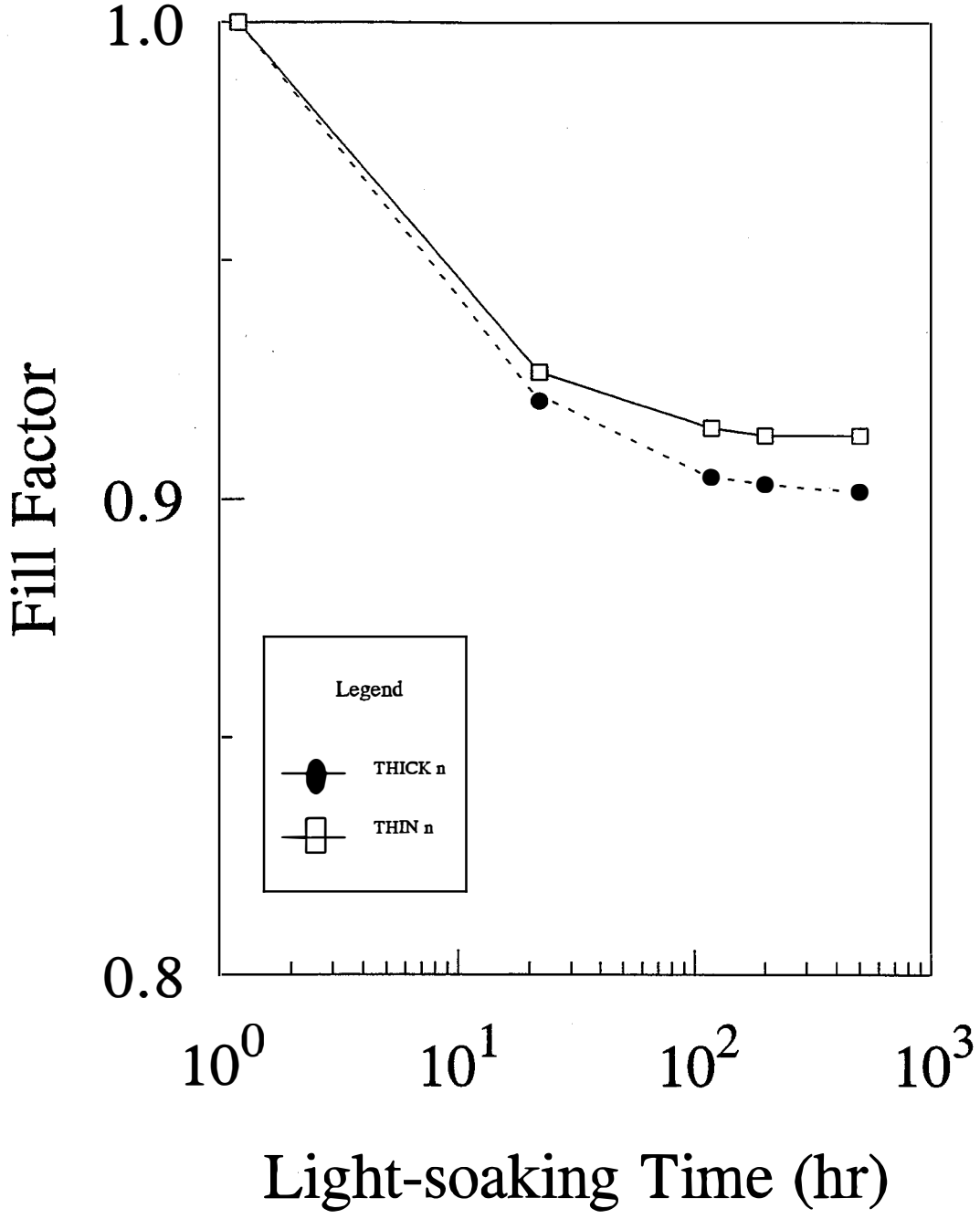

Figure 8. Normalized fill factor versus light-soaking time for two a-Si:H solar cells with thin and thick n-layers.

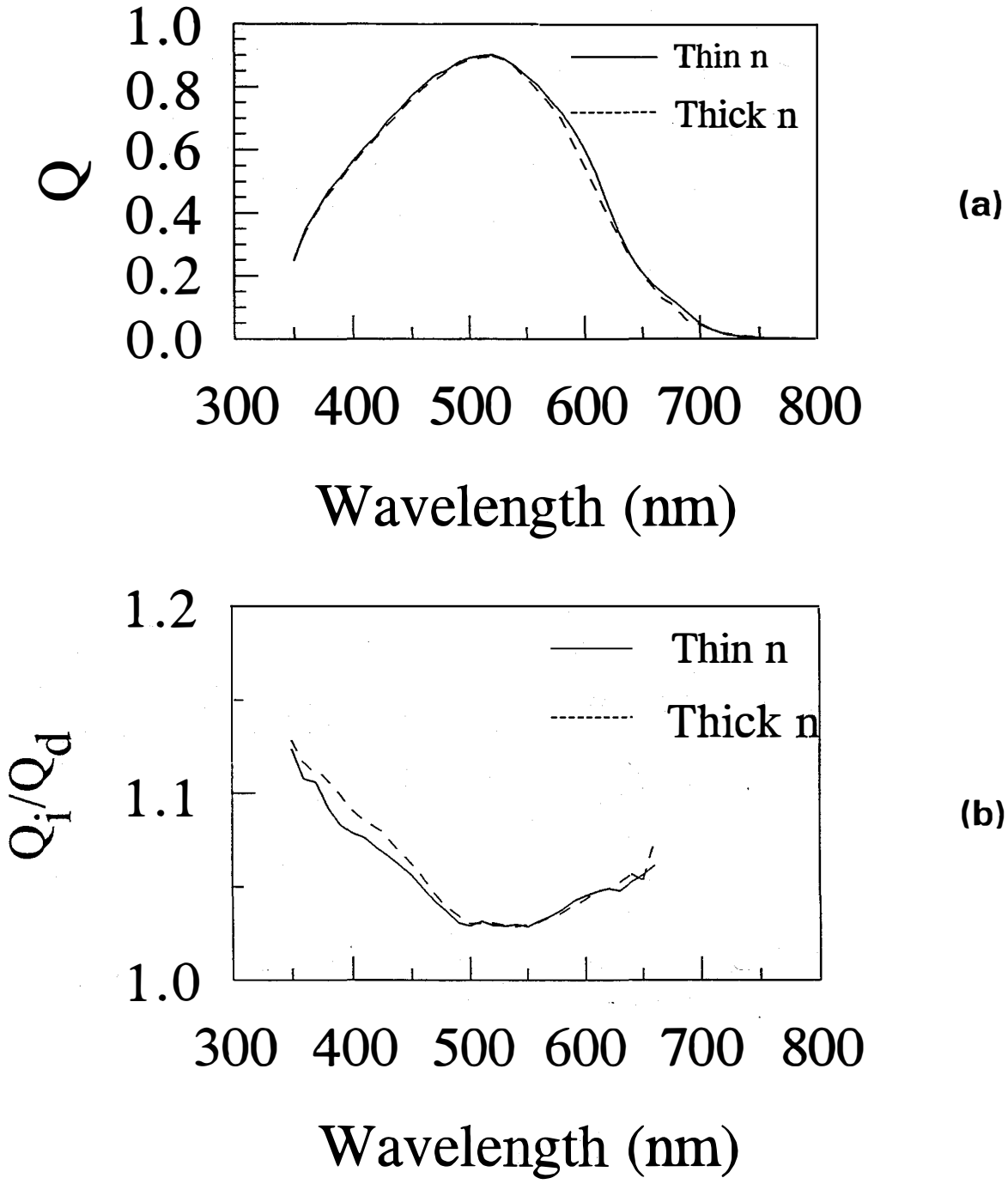

Figure 9. (a) Quantum efficiency of two degraded a-Si:H solar cells with thin and thick n-layers and (b) ratio of initial to degraded quantum efficiency of the two cells.

Section 6

Effect of μc-*n* Layer on a-Si:H/a-Si:H and a-Si:H/a-SiGe:H Double-junction Cells

Introduction

It is well known that microcrystalline (μc) boron-doped layer plays a key role in improving the efficiency of a-Si alloy solar cells. Compared to their amorphous counterpart, μc *p*-type layers show lower conductivity activation energy and higher optical transmission, giving rise to higher open-circuit voltage and short-circuit current for the solar cell. On the other hand, phosphorus-doped *n*-type amorphous silicon alloy films exhibit lower activation energy and higher transmission than *p*-type a-Si:H films; therefore, we have been using *n*-type a-Si:H layers in our multijunction cells.

In a continuous effort to improve the multijunction solar cell efficiency, we have examined the possibility of reducing light absorption caused by a-Si:H *n* layers and lowering contact resistance. Specifically, we have studied the effect of replacing the amorphous *n* layers by μc-*n* layers on the performance of multijunction cells by carrying out a set of experiments incorporating μc-*n* layers in the tunnel junction.

Effect of Microcrystalline *n* Layer in the Tunnel Junction of *n i p n* and $n_1i_1p_1n_2i_2p_2$ Structure

We have reported before that *n i p n* is a very effective structure to evaluate properties of tunnel junctions for multijunction a-Si alloy cells (Guha 1994). Therefore, our first experiment is to compare the properties of the $n_1i_1p_1n_2$ structure with an amorphous n_2 layer to that with a microcrystalline n_2 layer. To reduce the variation caused by the "bottom" cell, all the $n_1i_1p_1$ component cells were cut from the same sample deposited over 1 ft x 1 ft area (2B3857). The results on $n_1i_1p_1n_2$ structures are tabulated in Table 7. Two different recipes were employed to deposit μc-n_2 layers, i.e., low and high H_2 dilution. Compared with the sample with a-n_2 layer, the two samples with μc-n_2 layers show higher J_{sc}, V_{oc}, FF, and Q at 550 nm. It appears that μc-n_2 layers give rise to better performance than a-n_2 layers.

As a natural extension of the experiment described above, i_2 and p_2 layers were subsequently deposited on the top of the $n_1i_1p_1n_2$ structure to complete the a-Si alloy double-junction solar cell. Surprisingly, the double-junction a-Si alloy cells with μc-n_2 layers show lower V_{oc} than the cell with a-n_2 layer (see Table 8). To check if the thickness of the μc-n_2 layer was large enough for double-junction cells, thicker μc-n_2 layers were deposited for some double-junction cells. It turned out that thicker μc-n_2 layers resulted in lower V_{oc} for double-junction cells than thin μc-n_2 layers. In extreme cases, thick μc-n_2 layer deposited with high H_2 dilution reduced double-junction cell V_{oc} by as much as 160 mV.

We postulated that there could be some incompatibility between the μc-n_2 and i_2 layers, and a thin proprietary buffer layer is inserted between μc-n_2 and a-i_2 layers. Characteristics of the double-junction cells with such combined μc-n_2/buffer layers are also listed in Table 8. The values of V_{oc} of the double-juncton cells (#5403 and 5401) with μc-n_2/buffer layers are comparable to the cells with single a-n_2 layers (#5376 and #5402).

Experiments on $n_1i_1p_1n_2$ structure using the combination of μc-n_2 /buffer layers were performed to check whether there is still gain in Q. It is clear from Table 9 that the samples with combined μc-n_2/buffer layers show slightly higher values of Q at 550 nm, which indicates that the combined n_2 layers absorb less light than single a-n_2 layer (#5409).

We thus conclude that compared with amorphous *n* layers, μc-*n* layers have less absorption which reduces optical loss of the tunnel junction. Using a single μc-n_2 layer in the tunnel junction, double-junction cells show V_{oc} lowered by as much as 160 mV. The combination of μc-*n* and a thin buffer layer can provide the V_{oc} comparable to a-*n* layers with less absorption. Moreover, preliminary experimental results indicate that the combined μc-n_2/buffer layers may improve the quality of the tunnel junction in terms of lower contact resistance. We, therefore, decided to incorporate μc-*n* layers into the state-of-the-art multijunction cells.

Table 7. J-V Characteristics of $n_1i_1p_1n_2$ Structures.

Run #	J_{sc}	Q_{550}	V_{oc}	FF	Remarks
5369	11.2	0.70	0.916	0.592	a-n_2
5370	11.5	0.72	0.948	0.643	μc-n_2, Low H_2 dilution
5371	11.9	0.74	0.938	0.610	μc-n_2, High H_2 dilution

Table 8. Characteristics of a-Si:H/a-Si:H $n_1i_1p_1n_2i_2p_2$ Double-junction Structures.

Run #	V_{oc}	FF	Remarks
5376	1.804	0.652	a-n_2
5377	1.755	0.659	μc-n_2, Low H_2 dilution
5382	1.657	0.666	μc-n_2, High H_2 dilution
5384	1.782	0.640	μc-n_2, High H_2 dilution + buffer layer
5403	1.810	0.690	μc-n_2, High H_2 dilution + buffer layer
5401	1.819	0.645	μc-n_2, Low H_2 dilution + buffer layer
5402	1.797	0.636	a-n_2

Table 9. Q_{550} Characteristics of $n_1 i_1 p_1 n_2$ Structures.

Run #	Q_{550}	Remarks
5409	0.67	a-n_2
5408	0.70	μc-n_2, Low H_2 dilution + buffer layer
5410	0.71	μc-n_2, High H_2 dilution + buffer layer

Effect of Microcrystalline *n* Layer in the Tunnel Junction of Double-junction Cells

As we have discussed above, there appears to be an advantage in replacing the amorphous *n* layer in the tunnel junction with a combination of microcrystalline *n* layer with buffer layers. The motivation is to see if the combination structure can provide an improved optical property (less optical loss) and/or an improved electrical property (less electrical loss) in the tunnel junction of a multijunction structure.

We have carried out a series of experiments on a-Si:H/a-Si:H and a-Si:H/a-SiGe:H double-junction structures using conventional amorphous *n* layer and a combination of microcrystalline/ buffer layers in the tunnel junction. We have taken care to deposit the companion pairs onto the same back reflector; the pairs also have the same ITO deposited onto them. For the a-Si:H/a-SiGe:H structure, we have used middle cell/top cell parameters from a typical triple-junction structure. The J-V characteristics are listed in Table 10, and the quantum efficiency curves are shown in Fig. 10-13. It is observed that the double-junction cells with microcrystalline n_2/buffer layer in the tunnel junction give rise to higher efficiencies; the series resistance is lower and the quantum efficiency is higher. We will incorporate this approach in the triple structure.

Table 10. Characteristics of Double-junction Cells with Amorphous and Microcrystalline/Buffer *n* Layers in the Tunnel Junction.

Structure	*n* Layer in Tunnel Junction	J_{sc} (mA/cm^2)	V_{oc} (V)	FF	η (%)	Qtop/ Qbtm (mA/cm^2)	Qtotal (mA/cm^2)	R_s (Ω cm^2)
L8314 a-Si:H/a-Si:H	amorphous	7.80	1.901	0.752	11.15	7.97/ 7.8	15.77	15.0
L8317 a-Si:H/a-Si:H	microcrystalline/ buffer	8.06	1.919	0.766	11.85	8.06/ 8.28	16.34	14.3
L8375 a-Si:H/a-SiGe:H	amorphous	8.29	1.694	0.772	10.84	8.29/ 14.33	22.72	14.1
L8376 a-Si:H/a-SiGe:H	microcrystalline/ buffer	8.52	1.710	0.770	11.22	8.52/ 14.56	23.08	13.1

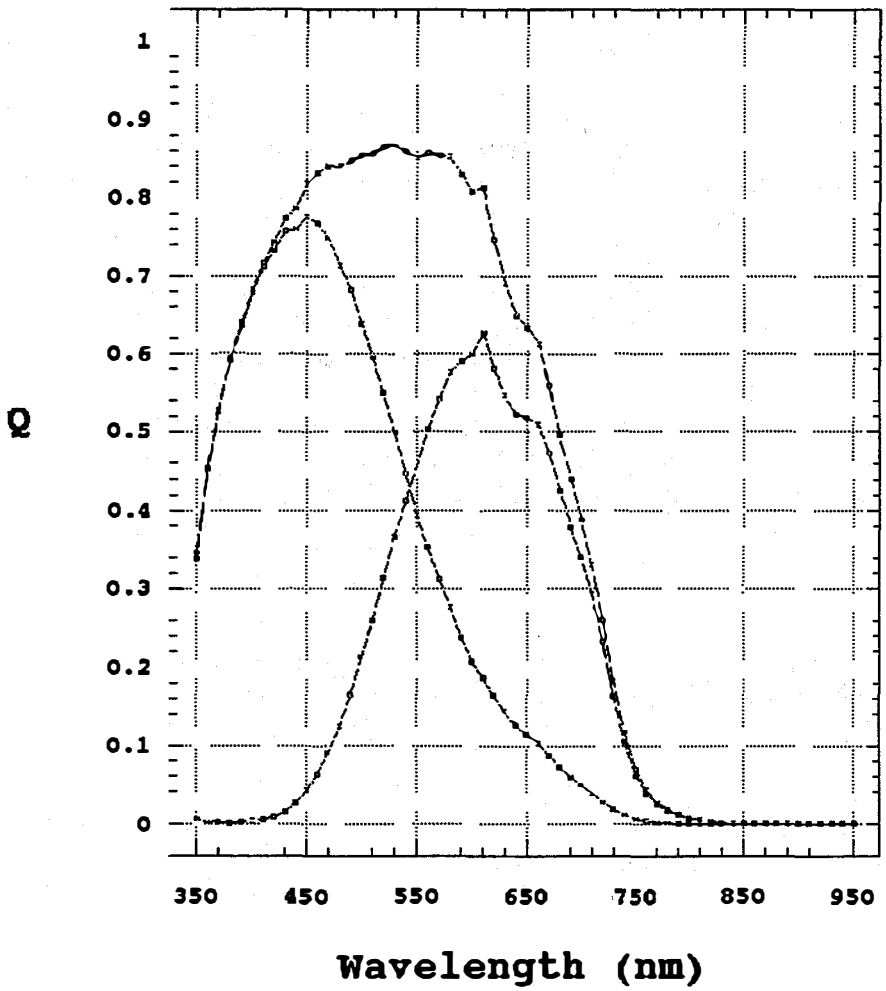

Figure 10. Quantum efficiency versus wavelength of an a-Si:H/a-Si:H double-junction cell (L8314) with amorphous *n* layer in the tunnel junction.

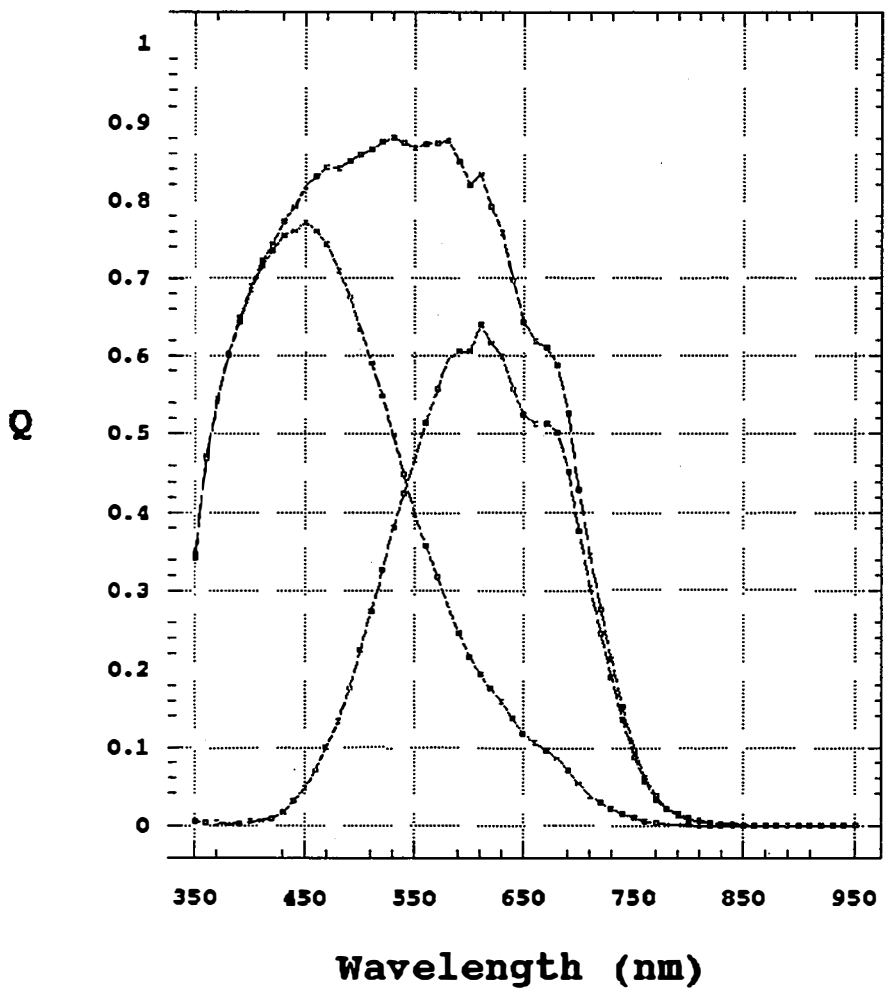

Figure 11. Quantum efficiency versus wavelength of an a-Si:H/a-Si:H double-junction cell (L8317) with microcrystalline *n*/buffer combination in the tunnel junction.

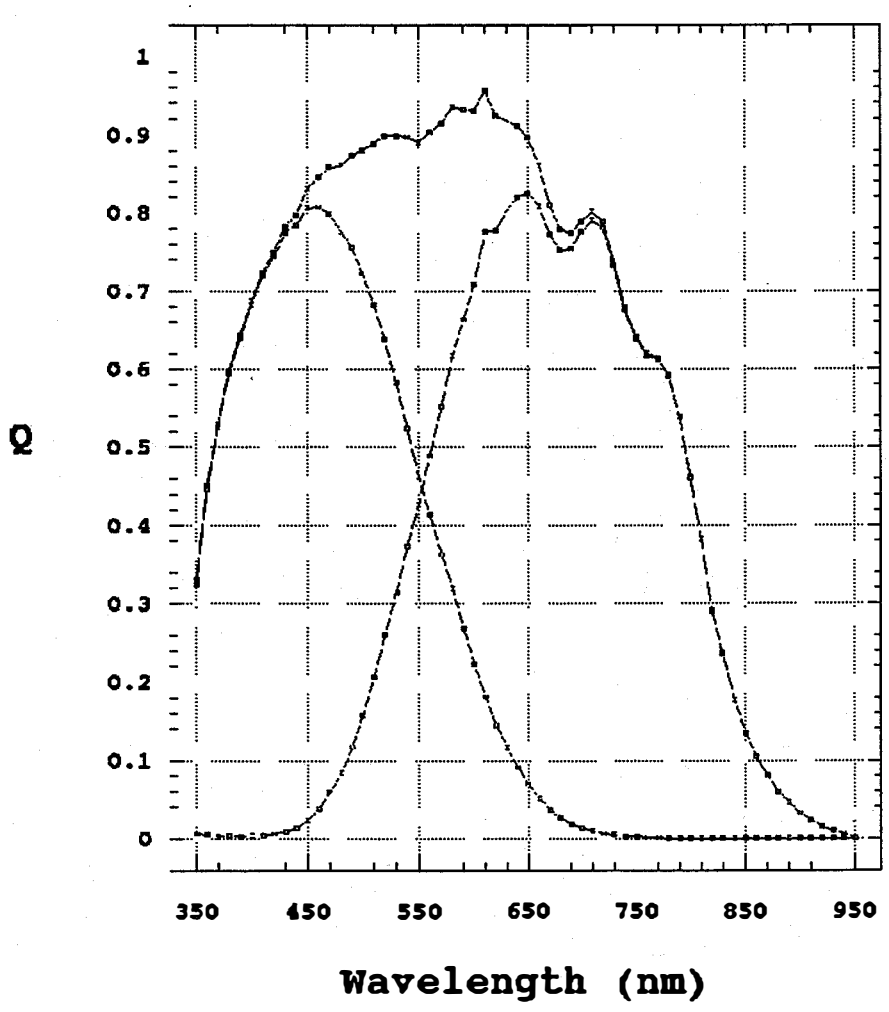

Figure 12. Quantum efficiency versus wavelength of an a-Si:H/a-SiGe:H double-junction cell (L8375) with amorphous *n* layer in the tunnel junction.

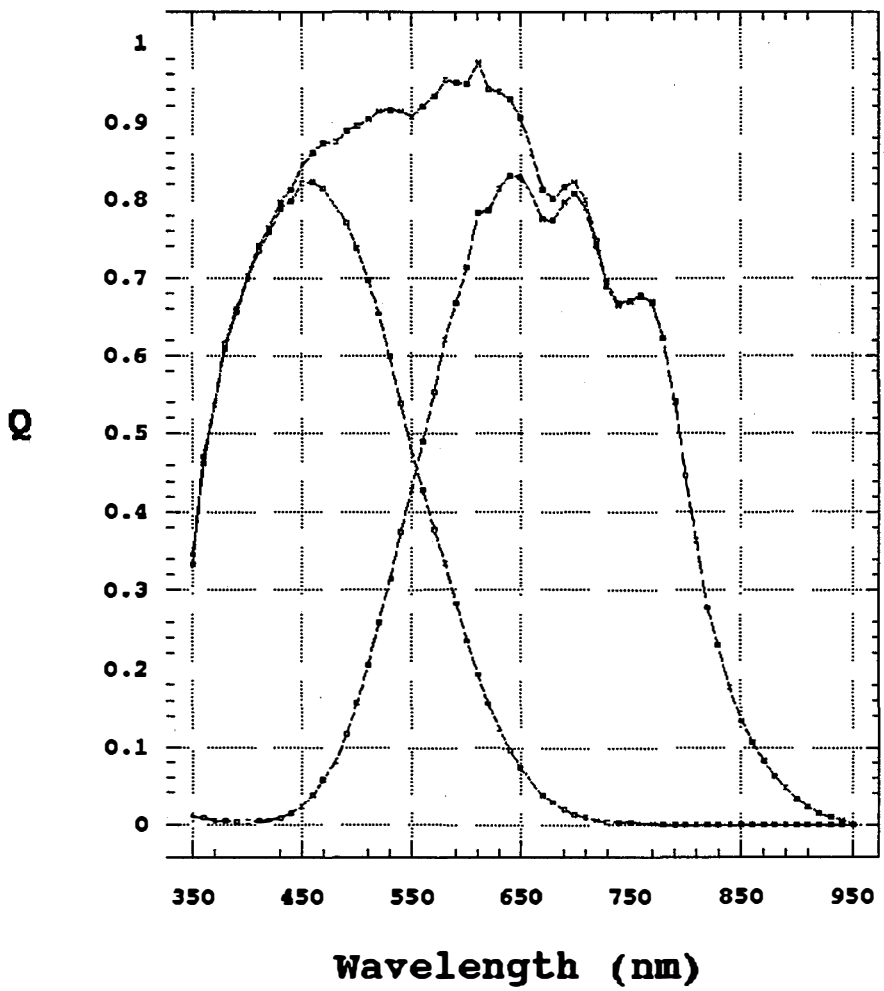

Figure 13. Quantum efficiency versus wavelength of an a-Si:H/a-SiGe:H double-junction cell (L8376) with microcrystalline *n*/buffer combination in the tunnel junction.

Section 7

Status of Component Cells and Triple-junction Performance

Introduction

In our Phase I Annual Technical Progress Report, we reported a stable active-area efficiency of 11.1% in a triple-junction cell of 0.25 cm^2 area. We have made substantial improvement during Phase II and achieved a world record of 11.8% stable efficiency in a triple-junction cell of 0.25 cm^2 area. This record efficiency was obtained after one-sun light soaking of the device for 1100 hours at 50 °C under open-circuit condition. A similar triple cell with a slightly lower performance was measured at NREL; a stable active-area conversion efficiency of 11.7% has been confirmed. This achievement is due to improvements made in the component cells as well as the design of component cell current mismatch. Details will be discussed in this section.

Experimental Results and Discussion

The basic structure of the triple junction has been reported previously (Yang et al. 1994) and shown in Fig. 14. It consists of ss/Ag/ZnO/$n_1i_1p_1$/ $n_2i_2p_2$/$n_3i_3p_3$/ITO, where i_1 and i_2 are a-SiGe alloys with different bandgaps and i_3 uses a-Si alloy. All devices have an active area of 0.25 cm^2 unless otherwise specified. Prior to this study, the highest stable triple cell efficiency was ~11%. Table 11 lists J-V characteristics for two such earlier triple cells. Both have an initial efficiency of ~13% and degraded to ~11% after 600 hours of one-sun, 50 °C light soaking. One can see from the quantum efficiency data that the current mismatch between the top and the middle cells is small (<0.1 mA/cm^2) in the initial state. In fact, it turned out that the middle cell became the current-limiting cell after degradation. Usually, the top cell is thin and has a better fill factor (Yang et al. 1994). It is therefore more desirable to limit the current by the top cell, especially after light soaking (Guha and Yang, U.S. Patent 1994). Furthermore, the total current from the sum of the component cells is ~22 mA/cm^2. In order to increase the mismatch among the component cells without sacrificing the triple-cell current, one must first develop a high-quality narrow bandgap bottom cell for producing enhanced red current.

One way to increase the red current is to increase the germanium content. This, however, often results in lower V_{oc} and FF. By optimizing deposition conditions including hydrogen dilution and bandgap profiling (Guha et al. 1989), we have obtained a narrower bandgap a-SiGe alloy cell with enhanced red response. The initial J-V characteristic is given in Table 12 along with our previous best result. It is readily observed that for λ >630 nm, the current density is increased from 9.91 mA/cm^2 to 11.9 mA/cm^2. The 2 mA/cm^2 increase represents a 20% gain in the red current. While V_{oc} is lowered as expected, the fill factor is only slightly poorer. The quantum efficiency for the narrower bandgap cell is shown in Fig. 15(a). Light soaking of the device was conducted in the same manner as described previously (Yang et al. 1994); the degradation versus light-soaking time is plotted in Fig. 16. The stabilized power is higher than our previous best value, also shown in Table 12. An a-SiGe:H cell with even more germanium incorporation is made. Its J-V characteristic is listed in Table 12.

For a given bottom cell, both the middle cell and the top cell need to be readjusted accordingly. In addition to the bandgap and thickness of the intrinsic layers, one also needs to consider the amount of current mismatch and the stability of the component cells. Optimization of the middle cell is usually done on bare ss substrates without back reflectors. However, it is interesting to compare the performance of

the middle and the bottom cells deposited on back reflectors. Figure 17 shows the J-V characteristic of an optimized middle cell deposited on ss/Ag/ZnO back reflector. The AM1.5 efficiency of 10.84% is believed to be the highest for an a-SiGe alloy cell. The quantum efficiency curve for this middle cell is plotted in Fig. 15(b). It is interesting to point out that this middle cell produces as much current as that produced by the bottom cell used in obtaining earlier triple cells in Table 11. The enhanced red response of the bottom cell is due to optimization of deposition conditions and increased germanium incorporation.

Table 11. Initial and Degraded Characteristics of Two Earlier Triple-junction Cells.

Sample No.	State	η (%)	J_{sc} (mA/cm^2)	V_{oc} (V)	FF	Q (mA/cm^2) Top	Mdl	Btm	Total (mA/cm^2)
Line 7358	Initial	13.0	7.16	2.45	0.74	7.16	7.20	8.38	22.74
	Degraded	11.1	6.87	2.38	0.68	6.98	6.87	7.97	21.82
	(600 h)	(-14.6)							
Line 7361	Initial	12.9	7.15	2.45	0.74	7.15	7.15	8.35	22.65
	Degraded	11.0	6.90	2.38	0.67	6.97	6.90	8.04	21.91
	(600 h)	(-14.7)							

Table 12. J-V Characteristics of the Previous, Recent, and Present Bottom Cells Deposited on Back Reflector and Measured under AM1.5 Illumination with a λ> 630 nm Filter.

Status	State	J_{sc} (mA/cm^2)	V_{oc} (V)	FF	P_{max} (mW/cm^2)
Previous	Initial	9.91	0.69	0.65	4.43
	Degraded	9.84	0.67	0.55	3.60
	(600 h)				(-18.7%)
Recent	Initial	11.9	0.61	0.63	4.57
	Degraded	11.4	0.60	0.56	3.80
	(600 h)				(-16.8%)
Present	Initial	12.5	0.59	0.63	4.64

As for the top cell, one would like to obtain high V_{oc} and high FF for a desired current density. Figure 18 shows a top cell with V_{oc} = 1.054 V, FF = 0.76, and J_{sc} = 6.2 mA/cm^2. The V_{oc} value of 1.054 V is the highest reported to date for an a-Si alloy cell with FF >0.75. For use as the top cell of a triple junction, one needs to increase the thickness of the intrinsic layer for obtaining a higher current density.

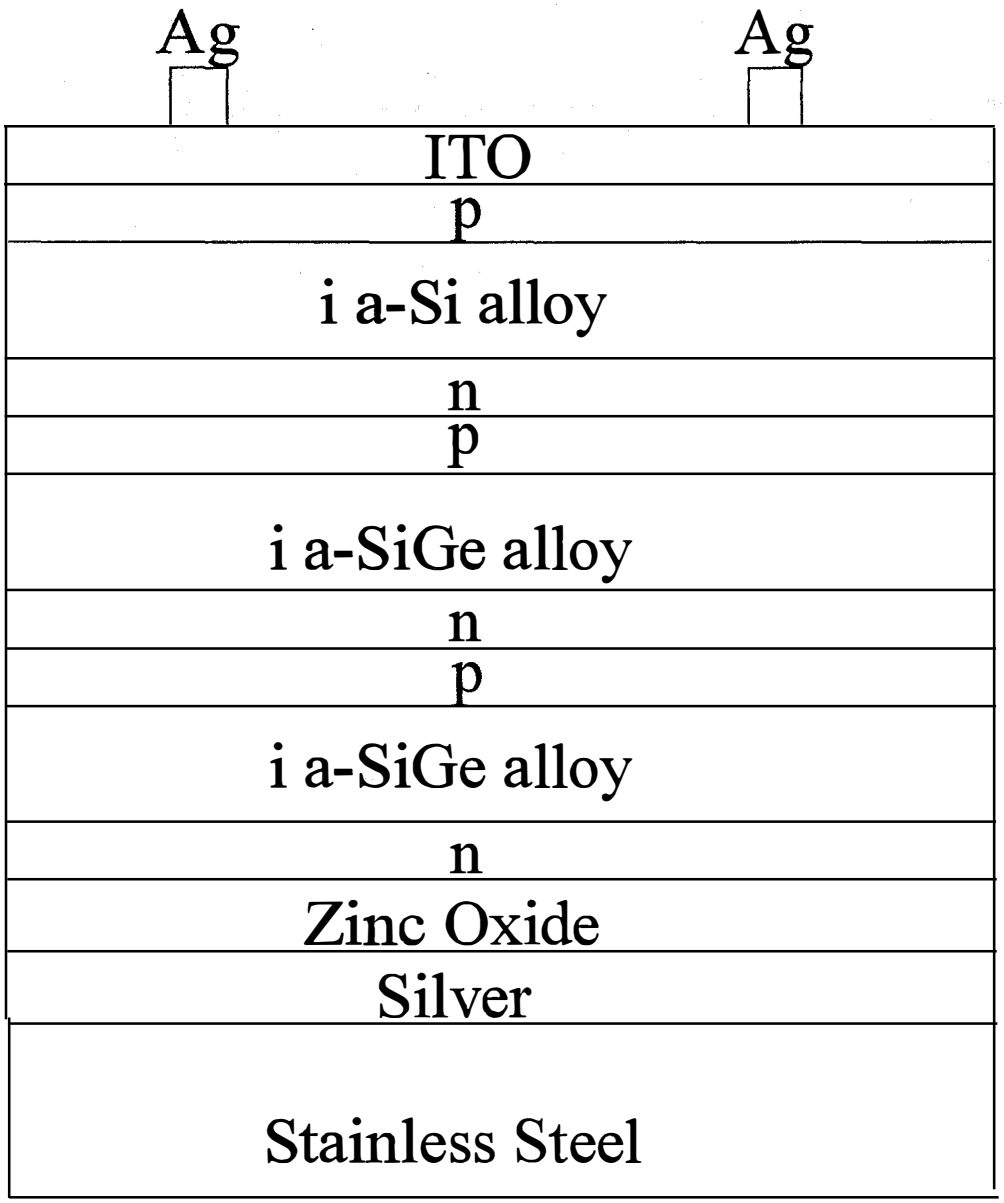

Fig. 14. Schematic diagram of triple-junction triple-bandgap device.

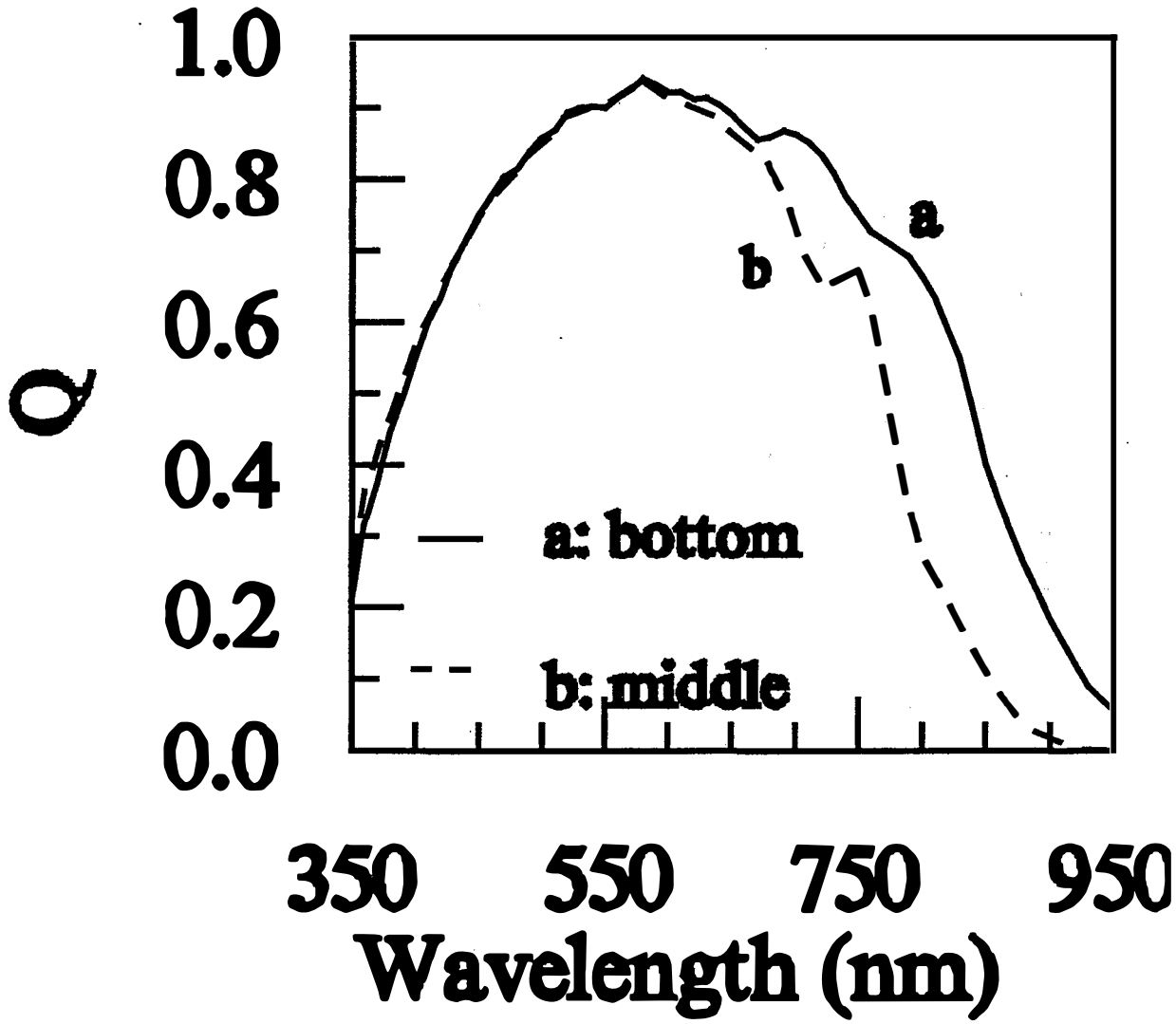

Figure 15. Quantum efficiency of a-SiGe alloy (a) bottom cell and (b) middle cell deposited on back reflector.

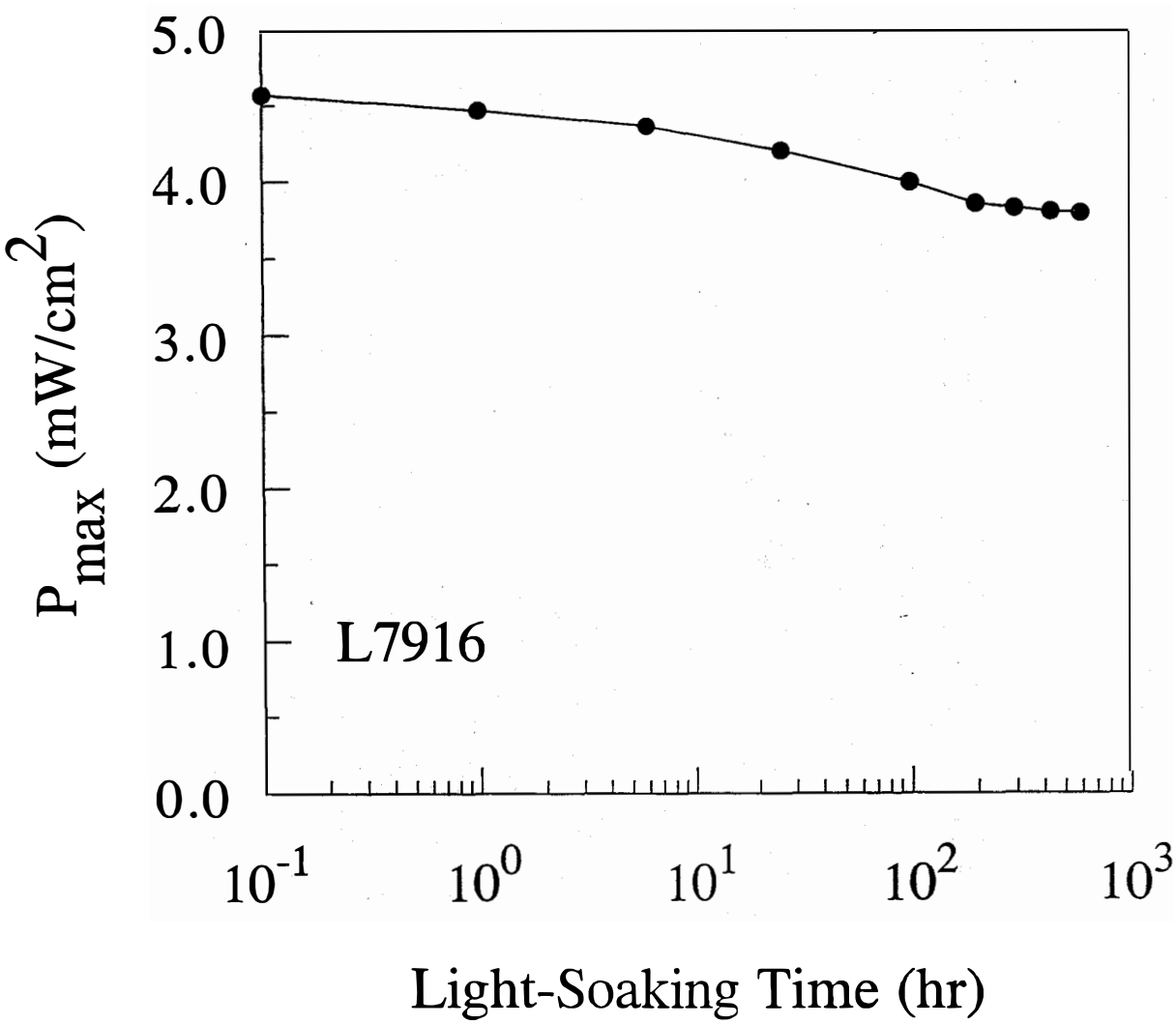

Figure 16. P_{max} versus light-soaking time for an a-SiGe:H narrow bandgap cell with a stabilized $P_{max} = 3.80 mW/cm^2$.

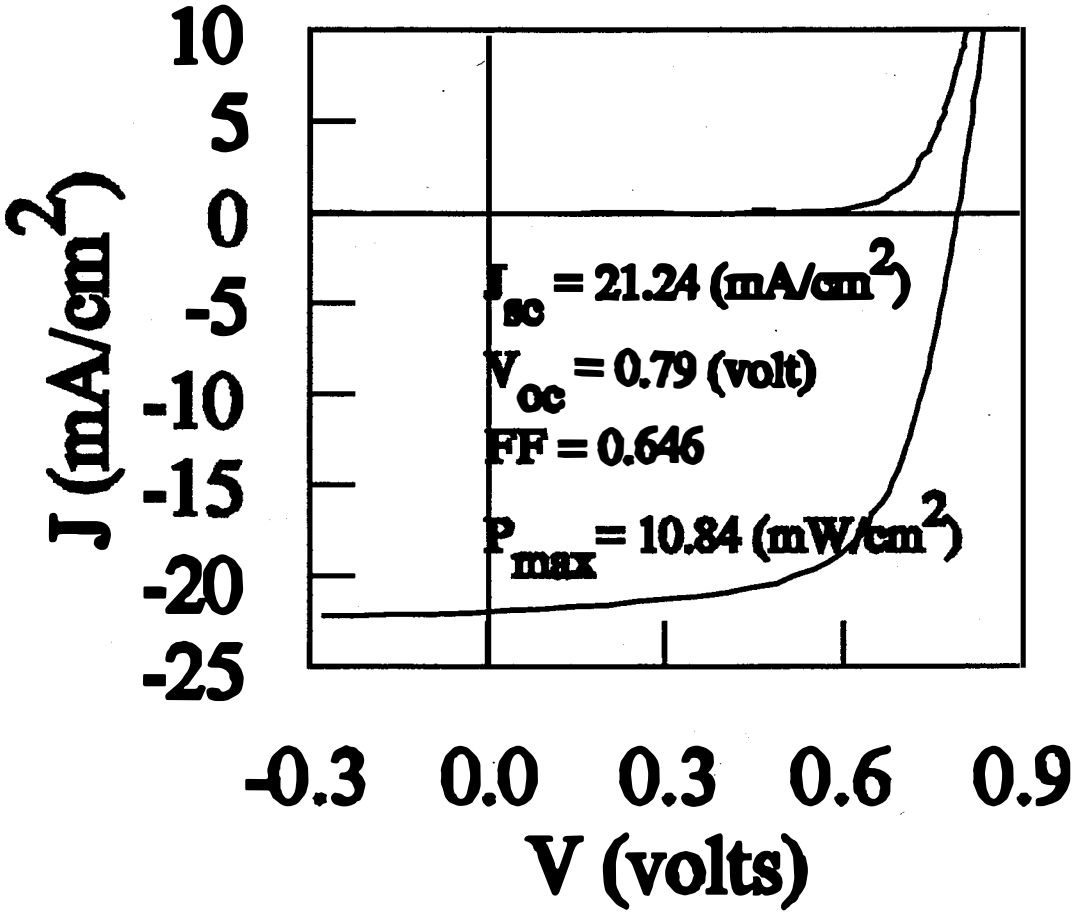

Figure 17. Initial J-V characteristic of an a-SiGe alloy middle cell deposited on back reflector.

Next we discuss the triple-junction design. For a given bottom cell, we first consider the desired current mismatch among the three component cells. Since the bottom cell gives rise to an enhanced red current and exhibits a total current density of ~25 mA/cm^2, a distribution of 7.6, 8.2, and 9.2 mA/cm^2 seems appropriate for the top, middle, and bottom cells, respectively. The larger mismatch allocated between the middle and the bottom cells takes into consideration the poorer fill factor of the bottom cell. The amount of mismatch between the top and the middle cells anticipates a slightly larger degradation of the middle cell and ensures the top cell to be the current-limiting cell after light soaking. We have used this design approach and fabricated triple cells and subjected them to one-sun, 50 °C, and open-circuit light-soaking condition. The degradation was substantially saturated at ~200 hours. After 600 hours of light soaking, we observed a true saturation. Some devices were sent to NREL for measurement. The best active-area efficiency was 11.7%, the highest confirmed to date. Some other devices were light soaked for a longer time. The best stable efficiency after 1100 hours is 11.8%, a new world record. The stabilized J-V characteristic and quantum efficiency curves are shown in Figs. 19 and 20, respectively. The effect of improved current mismatch on the performance of triple-junction cells is summarized in Table 13. Comparing characteristics in Tables 11 and 13, it is important to point out that in the degraded state, we now have the top cell as the limiting cell, consistent with our design principle. The degradation of the new design based on current mismatch is also improved significantly from 14.7% (Table 11) to 10.5% (Table 13). Incorporation of this design to large-area, one-square-foot module is underway. We should mention that we have seen very good correlation between indoor and outdoor measurements, and incorporation of these improvements in module design will give rise to better outdoor performance of modules as well.

Table 13. Characteristics of Improved Triple-junction Cells with Enhanced Current Mismatch.

Sample	State	J_{sc} (mA/cm^2)	V_{oc} (V)	FF	Q (mA/cm^2) Top	Mdl	Btm	Total (mA/cm^2)	United Solar* η (%)	Total Area (cm^2)	Active Area (cm^2)	NREL** η (%)
Line 7862	Degraded (600 h)	7.35	2.293	0.692	7.35	8.03	9.21	24.59	11.66	0.2668	0.2472	11.74
Line 7865	Degraded (600 h)	7.23	2.309	0.695	7.23	7.84	8.66	23.73	11.60	0.2664	0.2471	11.68
Line 7907	Initial	7.64	2.340	0.739	7.64	8.03	9.51	25.18	13.21			
	Degraded (1100 h)	7.49	2.283	0.692	7.49	7.77	9.33	24.59	11.83 (-10.5)			

* United Solar uses J_{sc} values as obtained from the quantum efficiency measurement.
** NREL result is based on converting total-area efficiency to active-area efficiency.

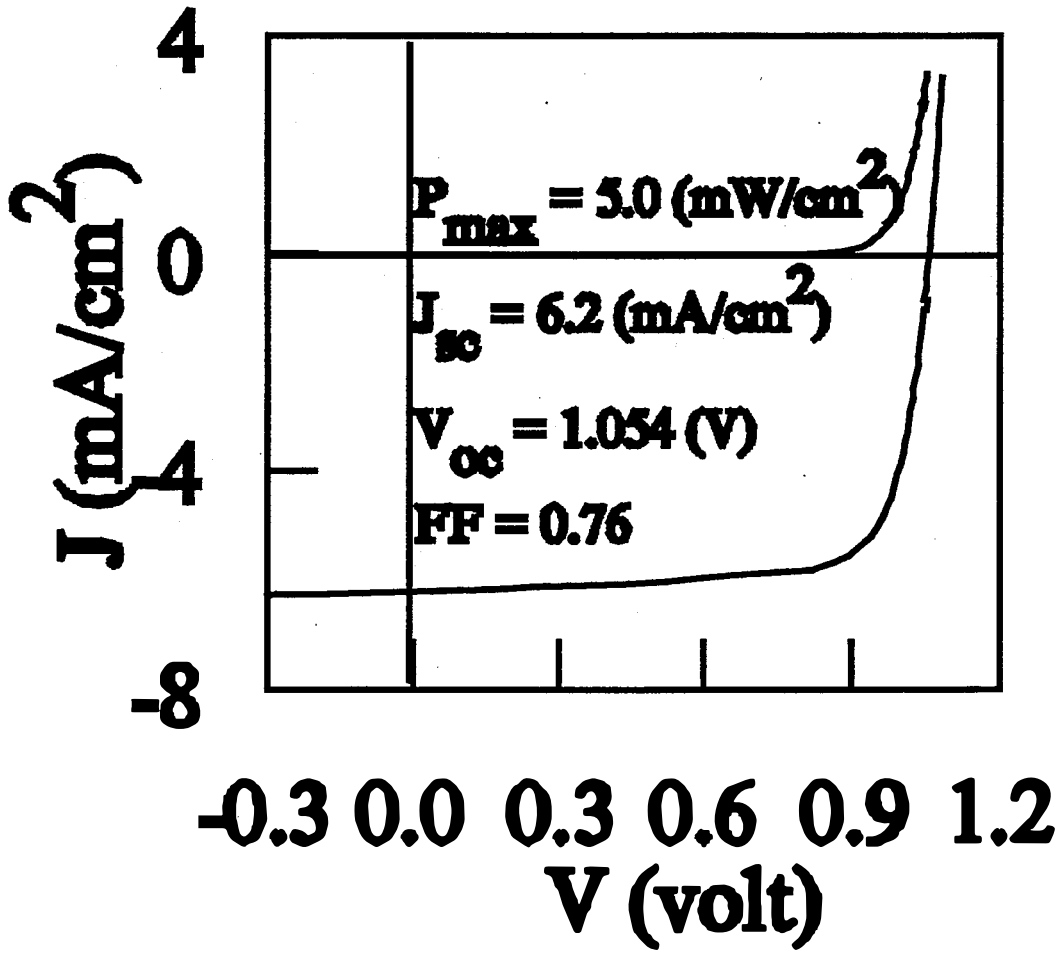

Figure 18. Initial J-V characteristic of a top cell on ss.

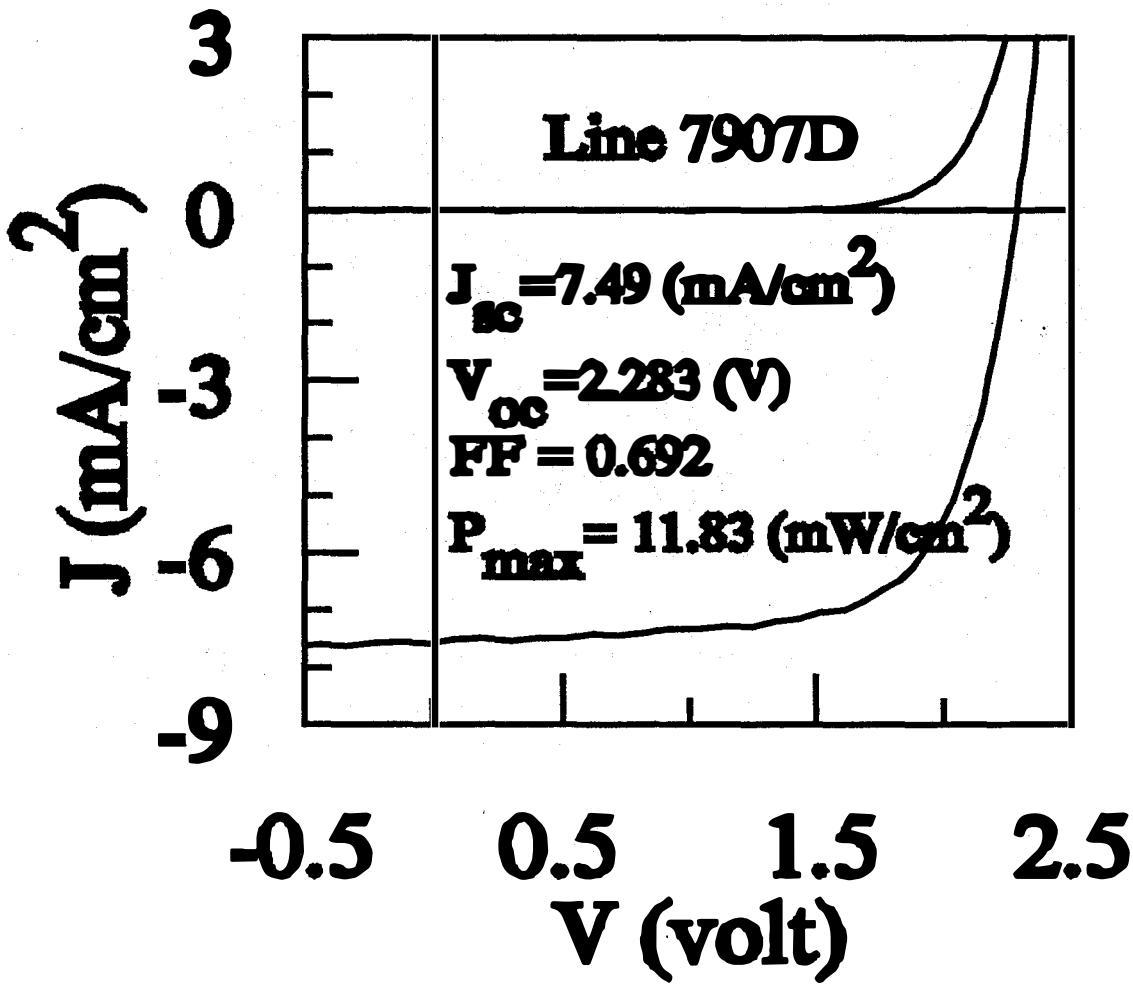

Figure 19. Stabilized J-V characteristic of the 11.8% cell.

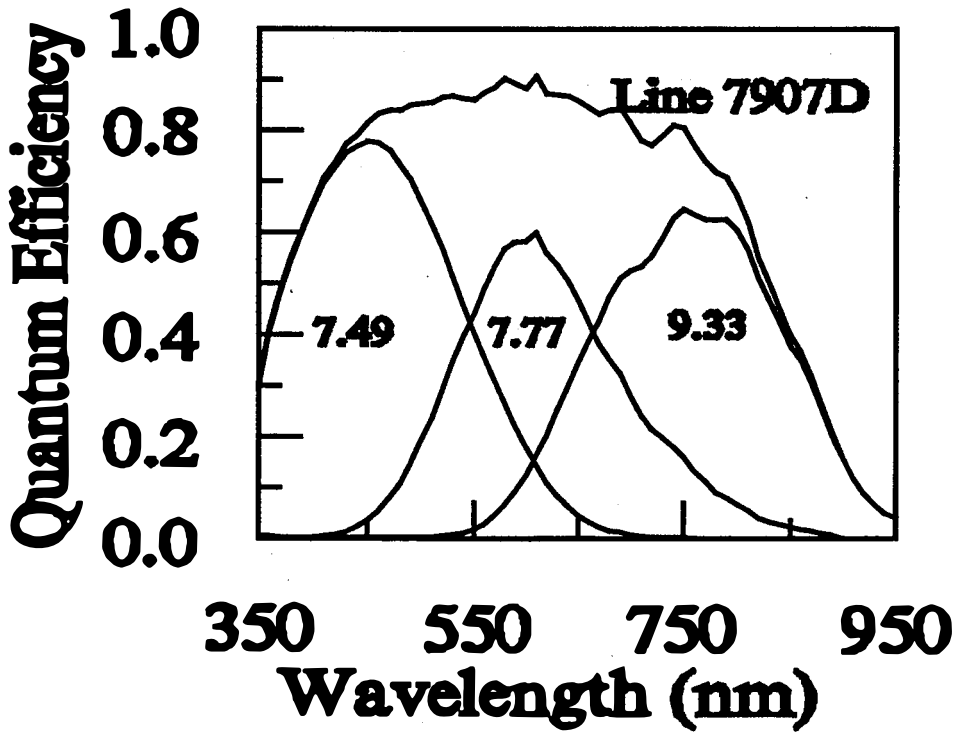

Figure 20. Quantum efficiency of the triple cell in Fig. 19.

Future Directions

Although significant progress has been demonstrated in Phase II of the program resulting in the achievement of world record efficiency of 11.83%, many challenges still remain to achieve the mid-term goal of 12% stable aperture-area module efficiency. As we had mentioned in our Phase I annual report, there is a need for identifying a new deposition regime to develop material of even higher quality. Many new deposition techniques are now being developed in different laboratories, and some of the methods have shown interesting results in terms of improved material property. It is extremely important to incorporate these materials in device configuration to assess their suitability for solar cells. There is a growing amount of evidence that structure of the material plays an important role in determining stability. Further work along this direction will also be rewarding. We shall continue to develop new materials in our laboratory and collaborate with others to obtain an improved understanding of the materials. Simultaneously, we shall also help other laboratories to put their material into device configuration so as to expedite progress. The collaborative efforts that have already been structured under the Thin Film Partnership will stimulate better understanding leading to devices with higher efficiency.

References

Dalal, V. L. (1995). NREL Quarterly Report, June-Aug.

Ganguly, G., Suzuki, A., Yamasaki, S., Nomoto, K., and Matsuda, A. (1990). *J. Appl. Phys.*; Vol. 68, p. 3738.

Ganguly, G., Yamasaki, S., and Matsuda, A. (1991). *Phil. Mag.*; Vol. B 63, p. 281.

Ganguly G. and Matsuda, A. (1994). *Phys. Rev. B*; Vol. 49, p. 10986.

Ganguly, G. and Matsuda, A. (1995). "A New Deposition Parameter that Controls the Carrier Drift Mobility in a-Si:H." Presented at the 16th International Conference on Amorphous Semiconductors, Kobe, Japan, 4-8 September.

Guha, S., Yang, J., Pawlikiewicz, A., Glatfelter, T., Ross, R., and Ovshinsky, S.R. (1989). "Band Gap Profiling for Improving the Efficiency of Amorphous Silicon Alloy Solar Cells." *Appl. Phys. Lett.*; Vol. 54, pp. 2330-2332.

Guha, S. (1993). *Research on Stable, High-efficiency Amorphous Silicon Multijunction Modules.* NREL/TP-411-5654. Golden, CO: National Renewable Energy Laboratory. Work performed by United Solar Systems Corp., Troy, Michigan.

Guha, S. (1994). *Research on Stable, High-efficiency Amorphous Silicon Multijunction Modules.* NREL/TP-411-7190. Golden, CO: National Renewable Energy Laboratory. Work performed by United Solar Systems Corp., Troy, Michigan.

Guha, S. (1995). *Amorphous Silicon Research.* Golden, CO: National Renewable Energy Laboratory. Work performed by United Solar Systems Corp., Troy, Michigan.

Lyding, J.W., Hess, K., and Kizilyalh, I.C. (1996). *Appl. Phys. Lett.*; Vol. 68, p. 2526.

Stuzmann, M., Jackson, W.B., Smith, A.J., and Thompson, R. (1986). *Appl. Phys. Lett.*; Vol. 48, p. 62.

Yang, J., Banerjee, A., Glatfelter, T., Hoffman, K., Xu, X., and Guha, S. (1994). "Progress in Triple-junction Amorphous Silicon-based Alloy Solar Cells and Modules Using Hydrogen Dilution." *First World Conference on Photovoltaic Energy Conversion Proceedings*, pp. 380-385.

REPORT DOCUMENTATION PAGE

Form Approved
OMB NO. 0704-0188

Public reporting burden for this collection of information is estimated to average 1 hour per response, including the time for reviewing instructions, searching existing data sources, gathering and maintaining the data needed, and completing and reviewing the collection of information. Send comments regarding this burden estimate or any other aspect of this collection of information, including suggestions for reducing this burden, to Washington Headquarters Services, Directorate for Information Operations and Reports, 1215 Jefferson Davis Highway, Suite 1204, Arlington, VA 22202-4302, and to the Office of Management and Budget, Paperwork Reduction Project (0704-0188), Washington, DC 20503.

1. AGENCY USE ONLY (Leave blank)	2. REPORT DATE	3. REPORT TYPE AND DATES COVERED
	October 1996	Annual Technical Progress Report, 1 August 1995 - 31 July 1996

4. TITLE AND SUBTITLE

Amorphous Silicon Research: Phase II; Annual Technical Progress Report, 1 August 1995 - 31 July 1996

5. FUNDING NUMBERS

C: ZAN-4-13318-02
TA: PV704401

6. AUTHOR(S)

S. Guha

7. PERFORMING ORGANIZATION NAME(S) AND ADDRESS(ES)

United Solar Systems Corp.
Troy, Michigan

8. PERFORMING ORGANIZATION REPORT NUMBER

9. SPONSORING/MONITORING AGENCY NAME(S) AND ADDRESS(ES)

National Renewable Energy Laboratory
1617 Cole Blvd.
Golden, CO 80401-3393

10. SPONSORING/MONITORING AGENCY REPORT NUMBER

SR-520-21964

DE96014327

11. SUPPLEMENTARY NOTES

NREL Technical Monitor: K. Zweibel

12a. DISTRIBUTION/AVAILABILITY STATEMENT

12b. DISTRIBUTION CODE

UC-1262

13. ABSTRACT *(Maximum 200 words)*

This report describes the progress made during the second year of a 3-year research program to improve our understanding and capabilities for developing multijunction, hydrogenated amorphous silicon alloy cells and modules. Highlights of the work include the investigation of new deposition regimes to control substrate bias during deposition, the substitution of hydrogen by deuterium to improve cell stability, the use of microcrystalline *n* layer to improve tunnel junction properties, and the development of high-efficiency component and multijunction cells. Progress has been demonstrated in the performance of all the component cells leading to the world-record achievement of 11.8% stable active-area cell efficiency using a triple-junction structure.

14. SUBJECT TERMS

photovoltaics ; amorphous silicon research ; multijunction cells ; hydrogenated amorphous silicon

15. NUMBER OF PAGES

46

16. PRICE CODE

17. SECURITY CLASSIFICATION OF REPORT	18. SECURITY CLASSIFICATION OF THIS PAGE	19. SECURITY CLASSIFICATION OF ABSTRACT	20. LIMITATION OF ABSTRACT
Unclassified	Unclassified	Unclassified	UL